

Supporting Information for

High efficient hydrogen evolution from seawater by a low-cost and stable CoMoP@C electrocatalyst superior to Pt/C

Yuan-Yuan Ma,^{‡a} Cai-Xia Wu,^{‡a} Xiao-Jia Feng,^a Hua-Qiao Tan,^{*a} Li-Kai Yan,^a Yang Liu,^b Zhen-Hui Kang,^{*b} En-Bo Wang^a and Yang-Guang Li^{*a}

^a Key Laboratory of Polyoxometalate Science of the Ministry of Education, Faculty of Chemistry, Northeast Normal University, Changchun, 130024, China. E-mail: liyg658@nenu.edu.cn; tanhq870@nenu.edu.cn.

^b Jiangsu Key Laboratory for Carbon-based Functional Materials and Devices, Institute of Functional Nano and Soft Materials (FUNSOM), Soochow University, Suzhou 215123, China. E-mail: zhkang@suda.edu.cn

section	page
Experiment Section	S2
Additional characterization techniques.	S2
Theoretical calculation methods	S3
Additional Figures of CoMoP@C.	S5
Additional Tables of CoMoP@C.	S30
Comparison of HER performance in acidic and alkaline media for CoMoP@C with other HER electrocatalysts.	S33
Additional experimental data for comparison	S36

1. Experimental Section

Chemicals and Reagents. Ammonium molybdate tetrahydrate ((NH₄)₆Mo₇O₂₄·4H₂O), Dicyandiamide (C₂H₄N₄, DCA) and Dextran (C_{6n}H_{10n}O_{5n}) were purchased from Aladdin Industrial Co., Ltd; Nafion solution (5 wt%), 20% and 40% Pt/C catalysts were purchased from Alfa Aesar China (Tianjin) Co., Ltd. All chemicals were used as received without further purification. The water (18.2 MΩ cm resistivity) used throughout all experiments was purified through a Millipore system. Phosphorus-rich polyoxometalate [Co(H₂O)₆]{[C₃H₄N₂]₂[C₅NH₅]₁₄[H₁₅(Mo₂O₄)₈Co₁₆(PO₄)₁₄(HPO₃)₁₀(OH)₃]}·5H₂O (Co₁₆Mo₁₆P₂₄) used as precursor was prepared according to the literature.^[1]

The preparation of control samples.

The preparation of CoMoP NPs: 0.1 g of Co₁₆Mo₁₆P₂₄ precursor was grinded into powder and directly annealed without adding DCA under the same condition. The obtained sample was labelled as CoMoP NPs.

The preparation of CoMoP@C with different thickness of carbon shell: the thickness of carbon shell was adjusted by the mass ratio of Co₁₆Mo₁₆P₂₄ and DCA. Two samples were synthesized under identical condition except that the mass ratio of Co₁₆Mo₁₆P₂₄ and DCA is 1:3 and 1:4. According to the results of TEM images (Figure S18), these two samples were denoted as CoMoP@C with the carbon shell thickness of 1.6-2.0 nm (CoMoP@C: 1.6-2.0 nm) and CoMoP@C with the carbon shell thickness of 2.6-3.8 nm (CoMoP@C: 2.6-3.8 nm), respectively.

The preparation of CoMoP@carbon: the synthetic procedure was similar to CoMoP@C except that the dextran was used instead of DCA.

The preparation of N doped C shell: N doped C shell was prepared by etching CoMoP@C catalyst in 4 M HNO₃ for 48 h with continuous ultrasonication. The etched sample was washed with deionized water and anhydrous ethanol for several times. Then, the obtained powder was dried in vacuum at 50 °C, which was defined as N doped C shell.

2. Additional Characterization techniques

Determination of Faradaic efficiency. The Faradaic efficiency of catalysts is defined as the ratio of the amount of experimentally determined H₂ to that of the theoretically expected H₂ from the reaction. The experiments were conducted in a typical airtight H-type cell with three-electrode configuration. In the experiments, the cathode and anode compartments were separated through a Nafion 117 proton exchange membrane. Before experiment, the electrolyte was bubbled with N₂ for at least 30 min. Then, the experiment was carried out. The gaseous product was analyzed by gas chromatography. As for the theoretical value, it was assumed that 100% current efficiency occurs during the reaction, which means only the HER process was occurring at the working electrode. The theoretical amount of H₂ evolved was then calculated by applying the Faraday law, which states that the passage of 96485.4 C charge causes 1 equivalent of reaction.

Proton Adsorption Measurements. The proton (H⁺) adsorption measurements were performed according to the method in literature.^[2] The concentration of 5 mM HCl solution

was selected and the adsorption experiments were conducted with a dialysis method. Typically, the CoMoP@C catalyst solution was dialyzed using a semi-permeable membrane (MWCO 1000) in a 600 mL beaker, and the dialysate was 5 mM HCl (500 mL). If CoMoP@C catalyst displays good adsorption behaviour for H⁺, H⁺ would gradually cross the semi-permeable membrane and dialyze into the CoMoP@C catalyst solution. After stirring on a shaker for predetermined time intervals, the residual concentration of HCl solution was determined by titrating with 5 mM NaOH solution.

The amount of adsorbed H⁺ (based on HCl), Q (g/g) is calculated by the following equation:

$$Q = \frac{(C_0 - C_e) \cdot V}{W}$$

Where C_0 and C_e are the initial and equilibrium concentration of HCl (mg/L), respectively; V is the volume of HCl solution (L) and W is the weight (mg) of CoMoP@C adsorbent.

3. Theoretical calculation methods

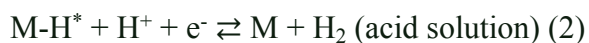
Theoretical analysis. From the kinetics and thermodynamics point of view, HER ($2H^+ + 2e^- \rightarrow H_2$) is a multi-step electrochemical process taking place on the surface of an electrode that generates gaseous hydrogen. Generally accepted reaction mechanisms in acid solutions are^[3-4]:

- 1) Electrochemical hydrogen adsorption (Volmer reaction) [Equation (1)]



Followed by

- 2) Electrochemical desorption (Heyrovsky reaction) [Equation (2)]



or

- 3) Chemical desorption (Tafel reaction) [Equation (3)]



Where H^* designates a hydrogen atom chemically adsorbed on an active site of the electrode surface (M). As indicated by reactions (1) and (2)/(3), chemical adsorption and desorption of H atoms on an electrode surface are competitive process. Theoretically, simple electrochemical redox reactions can be described by the Butler-Volmer equation^[5,6]:

$$j = j_0 \{ \exp(-\alpha f \eta) - \exp[(1-\alpha) f \eta] \}, \text{ (4)}$$

where α is the transfer coefficient, f denotes F/RT (F : the Faraday's constant, R : the universal gas constant, T : the absolute temperature), η defines the overpotential, which is the difference between the electrode and standard potentials ($\eta = E - E_0$), j denotes the current density, and j_0 is the exchange current density, a key descriptor of the electrocatalyst's activity. The equation represents the total currents from both reduction and oxidation reactions. First, we consider only forward rates that are sufficiently larger than the corresponding backward reaction rate. From the above equation, the following equation can be derived^[7]:

$$\eta = \frac{RT}{\alpha F} \ln(j_0) - \frac{RT}{\alpha F} \ln(j) \quad (5)$$

We now consider hydrogen evolution as a part of an electrochemical cell. During hydrogen evolution a current i will be running

$$i = -er \quad (6)$$

Where $r = r^+ - r^-$ is the net rate of hydrogen evolution reaction. An electric current is correlated with the reaction rate according to the following equation:

$$i = nFAr \quad (7)$$

or

$$j = nFr \quad (8)$$

Where i is the electric current, n is the number of electrons involved, and A denotes the surface area of the electrocatalyst, j is the current density. The kinetics in the process of HER may be complicated. The reaction velocity of hydrogen evolution may be written as^[13]:

$$r = ka_{H^+}[(1-\theta)^{1-\alpha}\theta^\alpha] \quad (9)$$

Here, r and k are the reaction rate and rate constant for Equation 9. a_{H^+} and θ denote the hydrogen ion activities and the surface coverage by the hydrogen atom, respectively. α is the charge-transfer coefficients ranging from 0 to 1.

The exchange current is the forward (and backward) rate when hydrogen evolution reaction is equilibrium. Combining Equation (8) and Equation (9), j_0 can be theoretically computed as an indirect function of $\Delta G(H^*)$

$$j_0 = Fk^0a_{H^+}[(1-\theta)^{1-\alpha}\theta^\alpha] \quad (10)$$

$$\theta = K/(1+K) \quad (11)$$

where

$$K = \exp(-\Delta G_{H^*}/k_B T) \quad (12)$$

Where K is the equilibrium constant, defined as the value of the reaction quotient at thermodynamic equilibrium, k_B is the Boltzmann constant. By relating the equations (5) to (12), the relationship between η , a_{H^+} and j can be expressed as:

$$\eta = Const + (RT/\alpha F) \ln(a_{H^+}) - (RT/\alpha F) \ln(j) \quad (13)$$

From the equation 13, the a_{H^+} around the catalyst has great influence on the activity of catalyst. As the H^+ concentration around the catalyst increases, the HER reaction rate will increase (Equation 9). For CoMoP@C catalyst, the strong adsorption proton capacity of N-doped graphitic carbon shell would enhance the proton concentration around CoMoP cores, thus resulting in the high HER performance of CoMoP, which might be superior to Pt/C.

DFT Computational Methods and Models. All DFT calculations within the frame of Vienna ab initio simulation package (VASP)^[8,9] were performed using the generalized gradient approximation (GGA) with the Perdew-Burke-Ernzerh of exchange correlation functional.^[10] A 350-eV cutoff energy was employed in all calculations and the convergence threshold for energy and force was set as 10⁻⁴ eV and 0.02 eV/Å, respectively. The interaction between the atomic cores and electrons was described by projector augmented wave method (PAW).^[11-12] The Brillouin zone was sampled with 3×3×1 Monkhorst-Pack k-point. In addition, the systems that involve Co were calculated with spin-polarization.

Figure S1 shows the model of CoMoP bulk, the lattice parameters are $a = 5.827 \text{ \AA}$, $b = 3.711 \text{ \AA}$ and $c = 6.780 \text{ \AA}$. In present work, CoMoP (112) surface is modeled. We have constructed the correlative theoretical models to investigate the HER activity of CoMoP@C composite (Figure S2). For comparative purpose, we also consider the composited CoMoP@Carbon (without N dopants), CoMoP, Carbon and N-doped C systems. The top three layers of CoMoP (112) and graphene were allowed to relax, while the rest of CoMoP (112) (the bottom

three layers) remained fixed. The corresponding lattice parameters used in the calculations have been presented in Table S1.

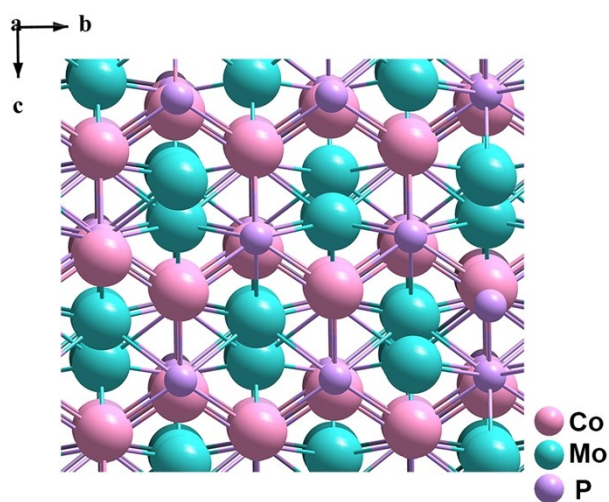


Figure S1. The ball and stick model of CoMoP. The CoMoP crystallized in the orthorhombic system, space group *Pnma*, with the lattice constants $a= 5.827(3) \text{ \AA}$, $b= 3.711(2) \text{ \AA}$, $c= 6.780(4) \text{ \AA}$.^[13]

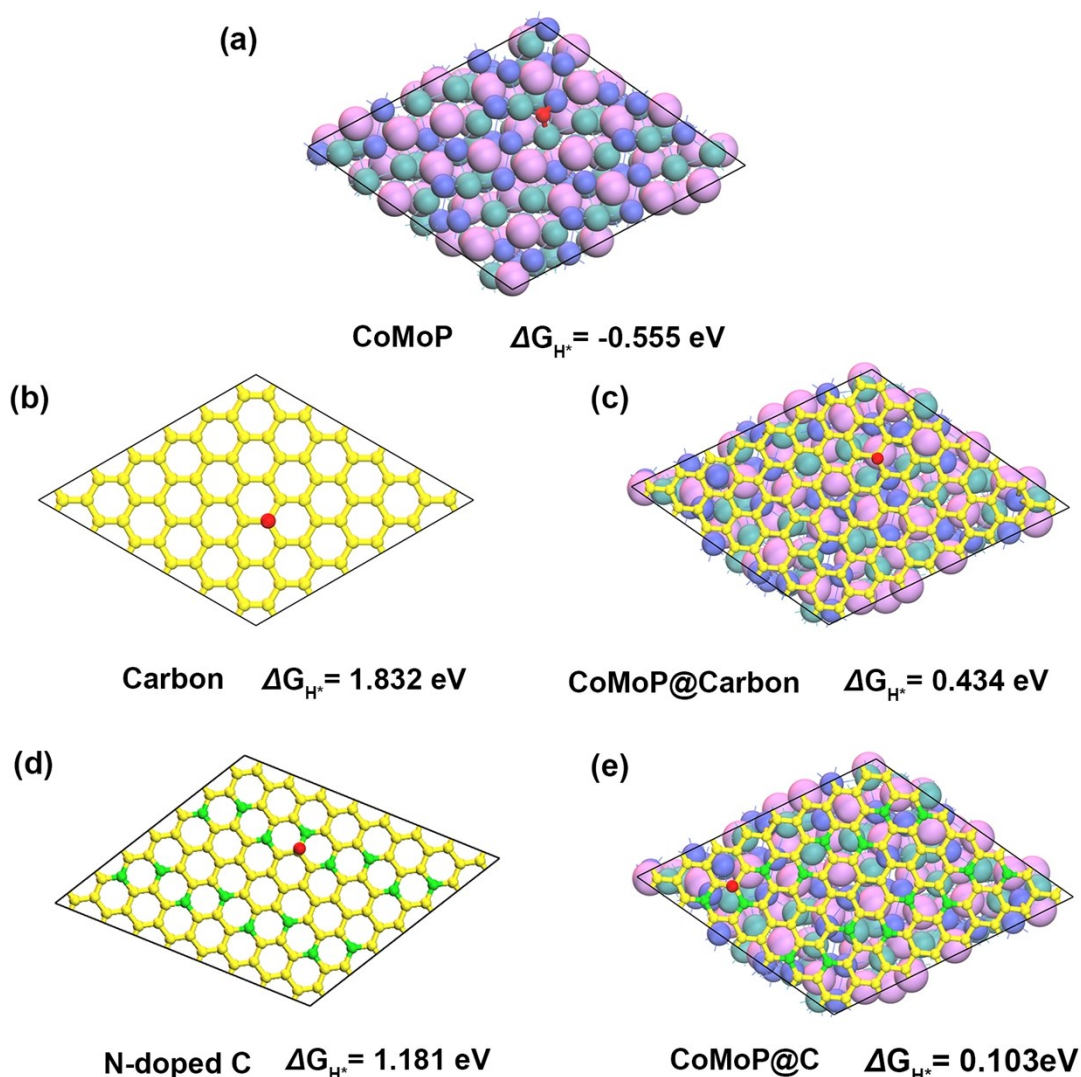


Figure S2. The theoretical models of H adsorbed on: (a) CoMoP, (b) Carbon, (c) CoMoP@Carbon, (d) N-doped C, (e) CoMoP@C. The yellow, green, violet, blueviolet, darkcyan and red balls represent C, N, P, Co, Mo and H atoms, respectively.

To compare the catalytic activity of different systems, the free energies of the intermediates were obtained by the equation $\Delta G(H^*) = \Delta E(H^*) + \Delta ZPE - T\Delta S$, where H^* denotes a H atom adsorbed on the surface and $\Delta E(H^*)$, ΔZPE and ΔS are the binding energy, zero point energy change and entropy change between the H adsorption and the gas phase, respectively. Therefore, ΔE_{ZPE} can be calculated as $\Delta E_{ZPE} = ZPE(H^*) - 1/2ZPE(H_2)$. The gas phase entropy of H was taken from the literature^[14]. Combining the analysis of Bader charge^[15] of atoms on the surfaces and the charge density difference (CDD) plotting (Figure S40), we selected several adsorption sites on each surface to investigate the capacity of H adsorption on different surfaces, involving one N atom (N site), several C sites adjacent to the N atom and one C site away from the N atom. The calculated binding energies, zero point energies and the free energies for H adsorption on different surfaces are listed in Table S2. It will be a good HER catalyst if $\Delta G(H^*) \approx 0$. The results indicate that the carbon atoms adjacent to N atom in CoMoP@C could possess considerably high activity for HER, which are corresponding to the blue area in the CDD picture of CoMoP@C (Figure S40).

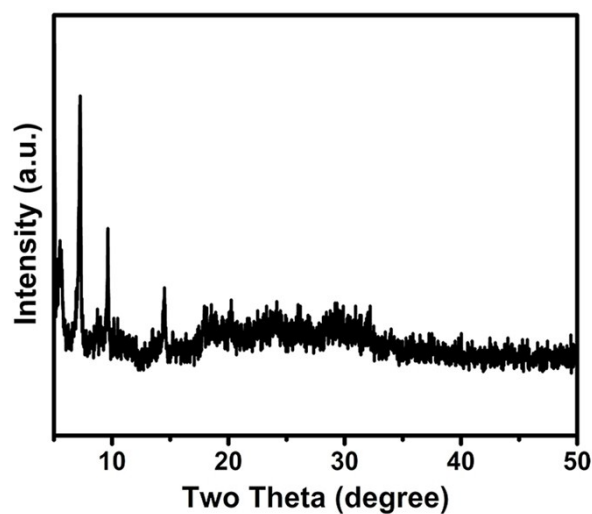


Figure S3. Powder XRD patterns of POMs precursor $\text{Co}_{16}\text{Mo}_{16}\text{P}_{24}$. The pattern of $\text{Co}_{16}\text{Mo}_{16}\text{P}_{24}$ is in agreement with the literature.^[1]

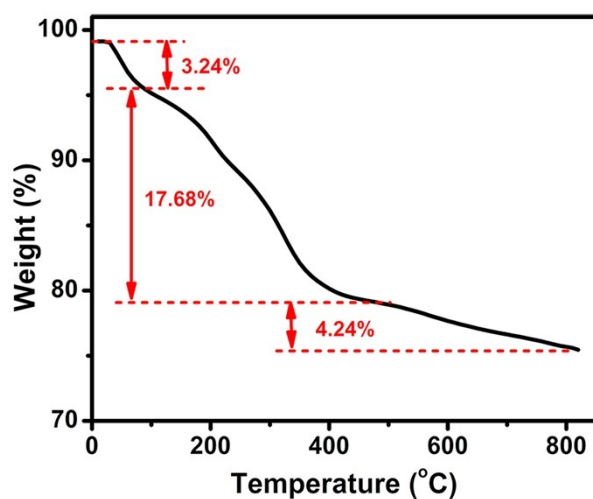


Figure S4. TG curve of $\text{Co}_{16}\text{Mo}_{16}\text{P}_{24}$. It shows a weight loss of 3.24% before 100 °C, corresponding to the release of coordinated and lattice water molecules. The second weight loss of 17.68% from 100 to 500 °C is attributed to the removal of all imidazole and pyridine ligands. The third weight loss of 4.24% in the temperature range of 500-800 °C may be attributed to the decomposition of partial P_2O_5 derived from the polyanion.

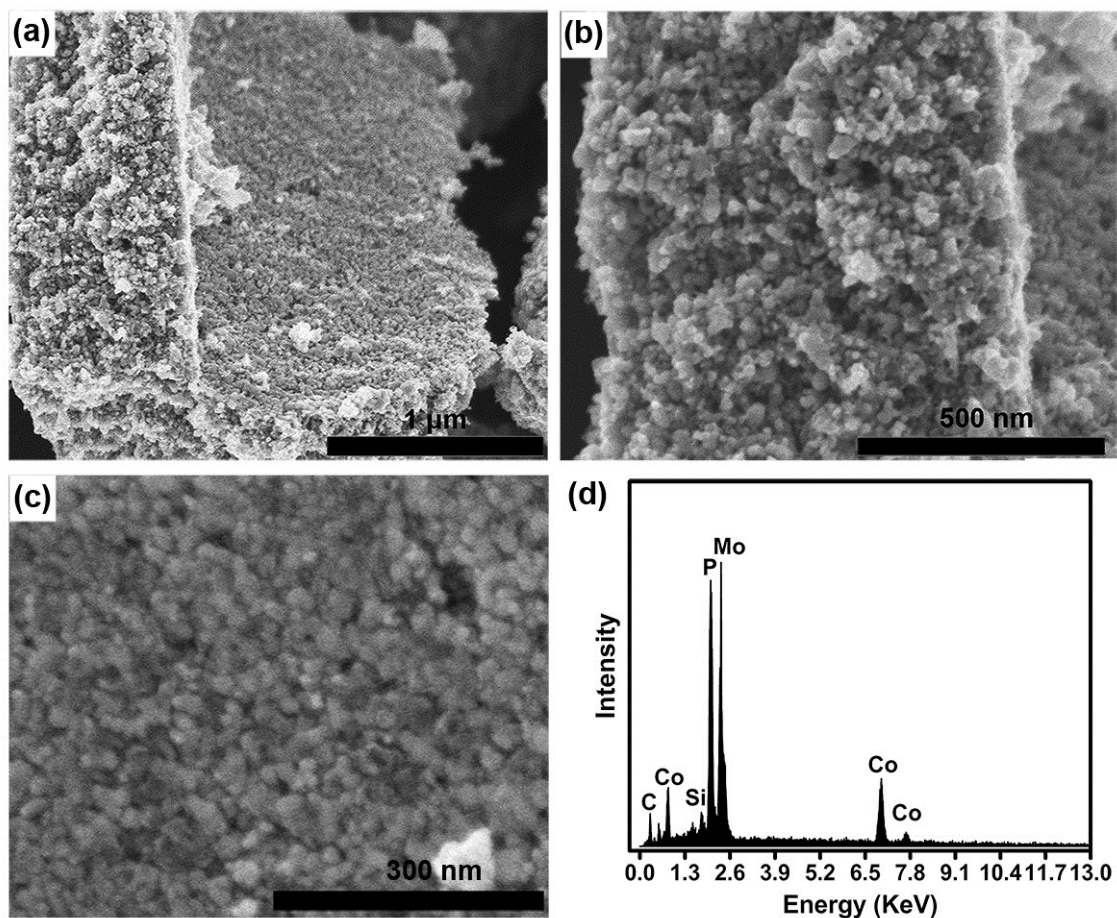


Figure S5. (a)-(c) SEM images of CoMoP@C annealed at 800 °C for 6 hour under N₂ atmosphere. The images show that as-synthesized superstructure is assembled from CoMoP@C nanoparticles of ca. 5-20 nm in diameter, which is in accordance with the results in TEM (5-20nm). (d) EDX spectra of CoMoP@C, demonstrating the catalyst consists of Co, Mo, P, C, N and O elements.

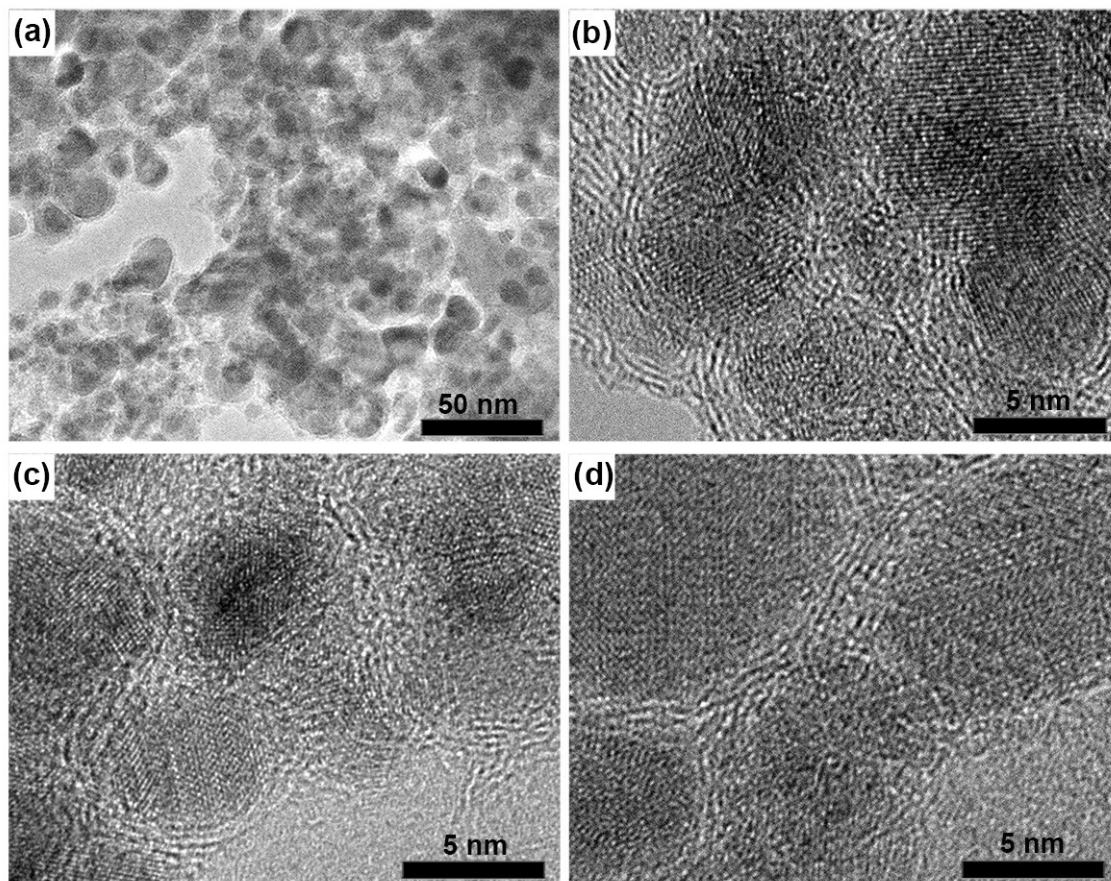


Figure S6. (a)-(d) Supplementary TEM images of CoMoP@C. TEM images indicate that the CoMoP particles are coated by graphene-like carbon shells with the thickness of 0.8-1.2 nm.

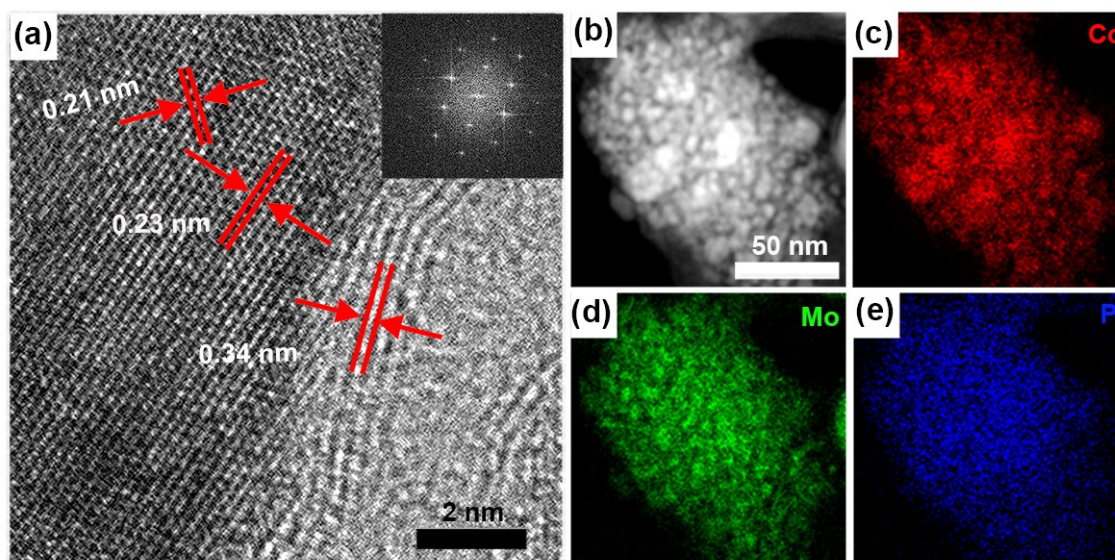


Figure S7. (a) High-resolution TEM images of CoMoP@C. Inset: the fast Fourier transform of lattice fringes of CoMoP core, indicating the single crystalline structure of CoMoP core. (b) High-angle annular dark field scanning TEM (HAADF-STEM) image of CoMoP@C. (c)-(e) its corresponding energy dispersive spectroscopy (EDS) mapping, indicating the spatial

distribution of Co (red), Mo (green) and P (blue), respectively. These results show that Co, Mo, P, C and N elements are evenly distributed on the surface of CoMoP@C.

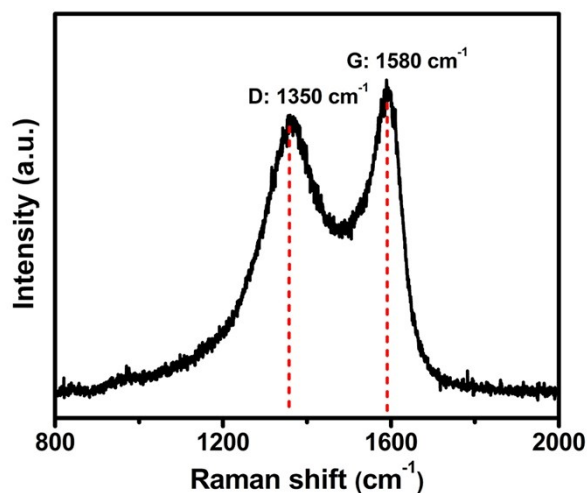


Figure S8. Raman spectrum of CoMoP@C with $I_D/I_G=2.16$, implying the presence of partial graphitization and many structural defects on carbon shells, thus favoring the electroconductivity and H⁺/H₂ adsorption.

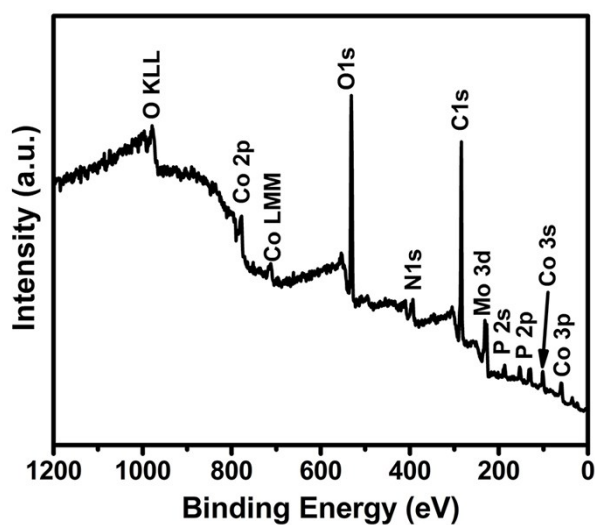


Figure S9. Full-scan XPS spectrum of CoMoP@C. Full-scan XPS spectrum indicates that the catalyst consists of carbon, nitrogen, oxygen, phosphorus, cobalt and molybdenum elements.

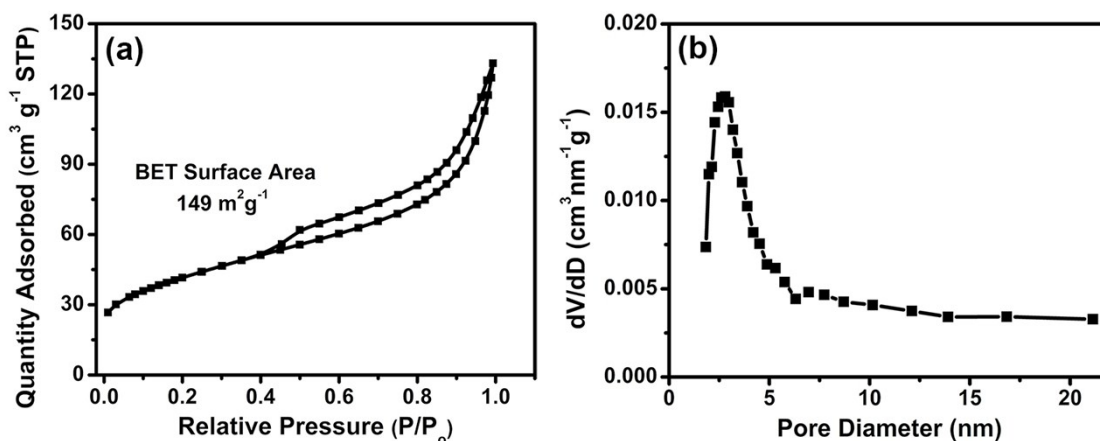


Figure S10. (a) N_2 sorption isotherms of CoMoP@C, which presents a typical IV hysteresis loop and the BET surface area is $149 \text{ m}^2 \cdot \text{g}^{-1}$. (b) The corresponding pore size distribution curves, indicating that the material possesses a mesoporous structure.

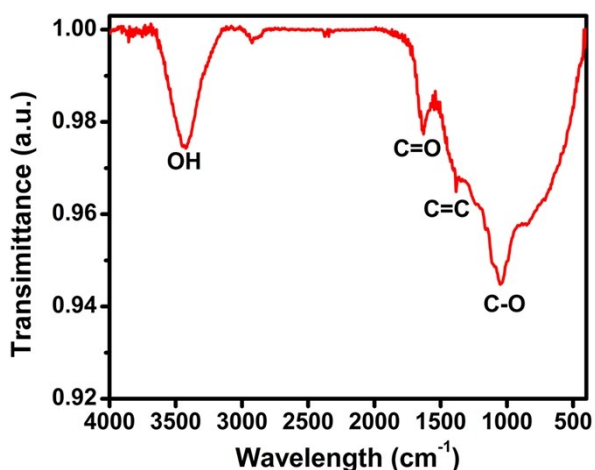


Figure S11. Fourier transform infrared (FTIR) spectra of CoMoP@C. The characteristic absorption band at $\sim 3435 \text{ cm}^{-1}$ can be attributed to the vibrations of O-H, and the peaks at ~ 1634 and $\sim 1380 \text{ cm}^{-1}$ are related to the vibrational stretching of C=O and C=C bonds. All of the above FTIR results indicate that the surfaces of CoMoP@C are full of hydrophilic groups (hydroxyl and carboxylic groups).

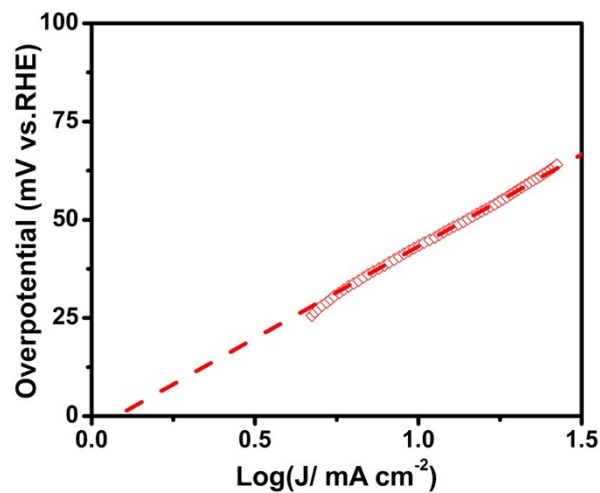


Figure S12. Calculation of exchange current density of CoMoP@C in 0.5 M H₂SO₄. The exchange current density (j_o) was calculated using extrapolation methods. When the overpotential value is 0, the log(j) value for CoMoP@C is 0.084, respectively. Based on Tafel equations, j_o for CoMoP@C was calculated to be 1.21 mA/cm².

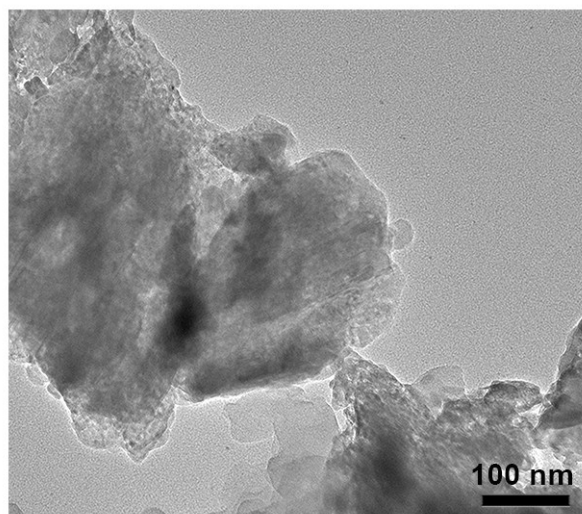


Figure S13. The TEM image of N-doped C shell. The image shows that most of CoMoP particles have been etched.

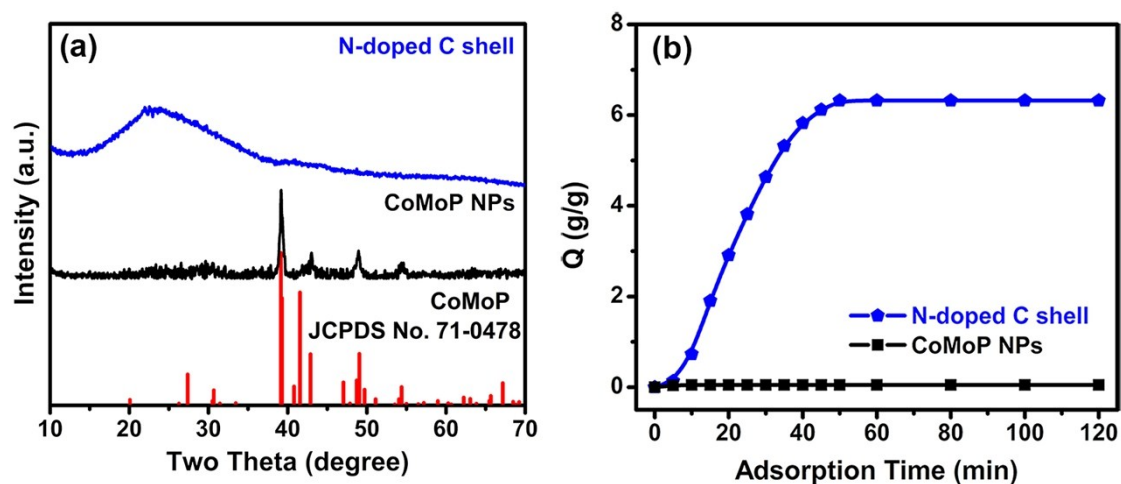


Figure S14. (a) The XRD patterns of N-doped C shell and CoMoP NPs. (b) Dependence of adsorption time on the amounts of adsorbed H^+ on N-doped C shell and CoMoP NPs in 5 mM HCl aqueous solution. The maximum H^+ adsorption capacity (based on the quality of HCl) are about 6.31 and 0.06g/g, respectively. These results indicate that the high proton adsorption capacity of catalysts may be attributed the N-doped carbon shell.

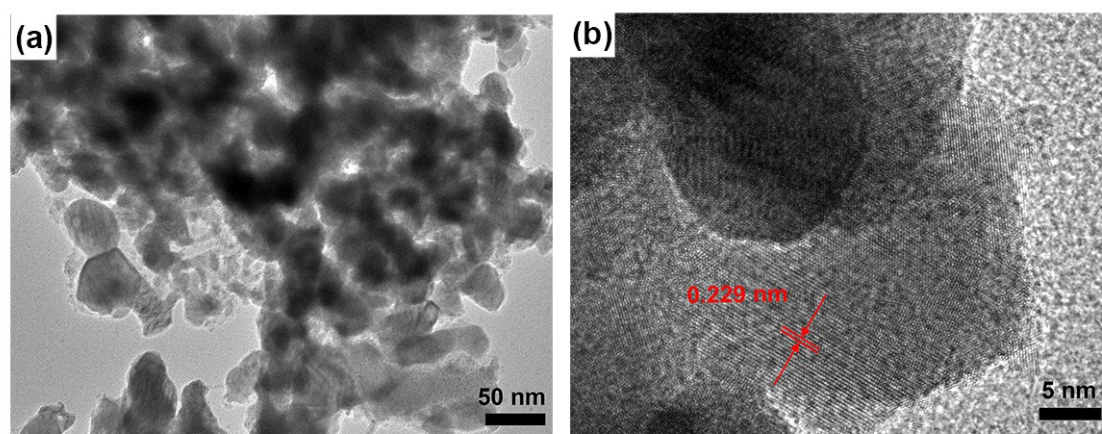


Figure S15. (a) The TEM image of CoMoP NPs. (b) The high-magnified TEM image of CoMoP NPs. The images show that CoMoP NPs tend to agglomerate during the heat treatment to form large aggregates, which decreases the exposed active surface. High-resolution TEM images reveal that no graphene-like carbon shells are observed on the surface of CoMoP NPs, which might result from the low carbon content of $Co_{16}Mo_{16}P_{24}$ precursors.

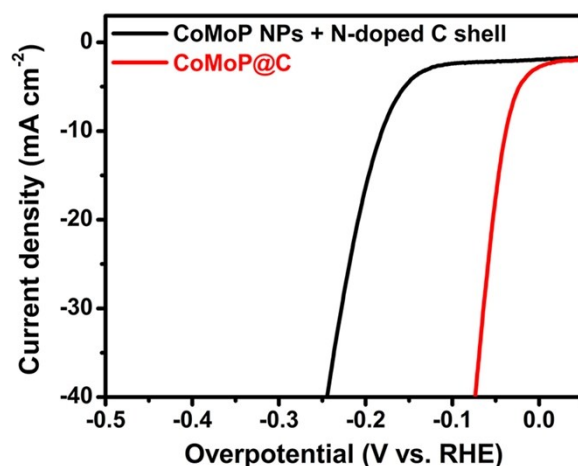


Figure S16. The HER polarization plots of CoMoP@C and the physical mixture of CoMoP NPs and N-doped C shell in 0.5 M H₂SO₄ at scan rate of 5 mV s⁻¹.

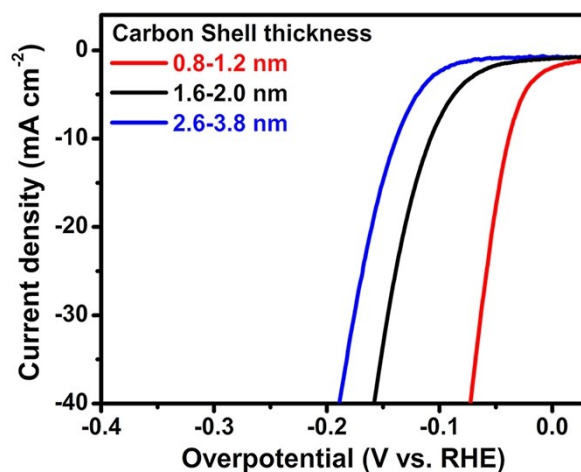


Figure S17. The HER polarization curves of CoMoP@C, CoMoP@C with the carbon shell thickness of 1.6-2.0 nm and CoMoP@C with the carbon shell thickness of 2.6-3.8 nm in 0.5 M H₂SO₄ at scan rate of 5 mV s⁻¹. The results show that the thickness of carbon shell has great influence on the HER activity of catalyst. The HER activity declines with the increase of the carbon shell thickness, which could affect the penetration of electrons during the HER process.²⁰

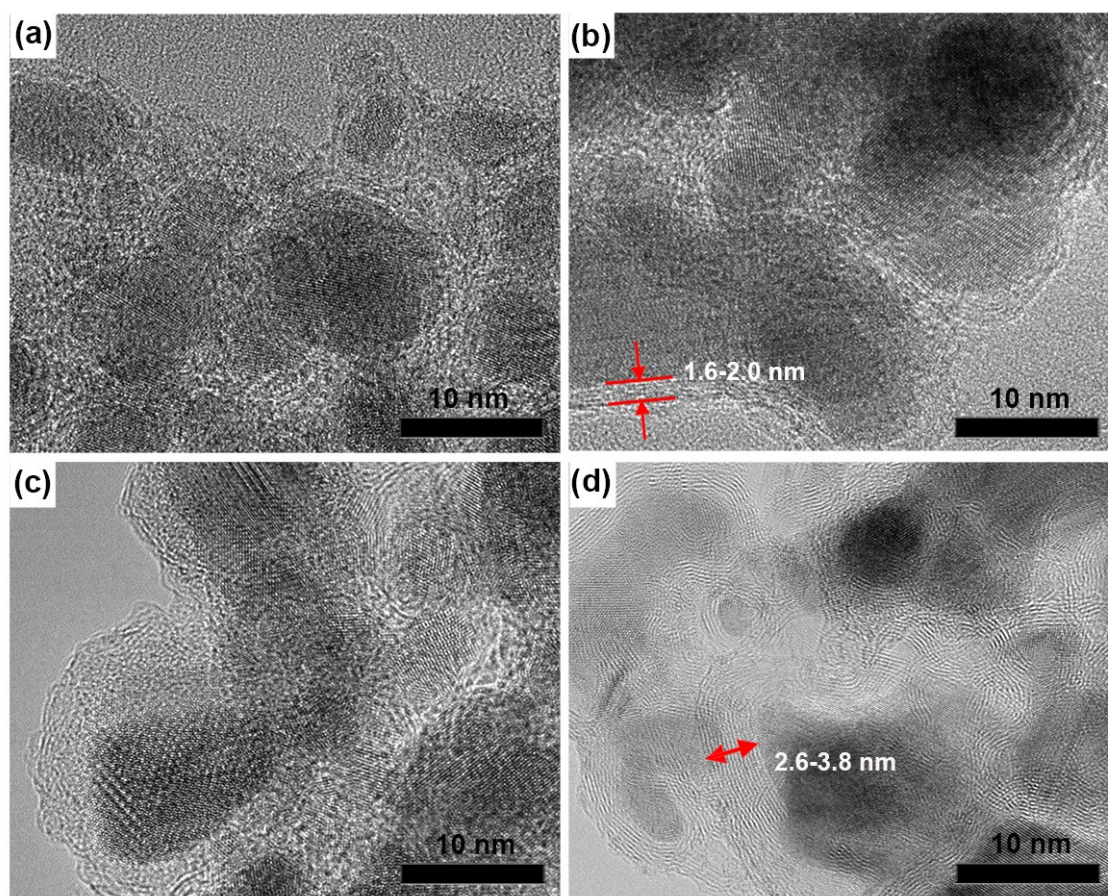


Figure S18. (a) and (b) TEM images of CoMoP@C with the carbon shell thickness of 1.6-2.0 nm. (c) and (d) TEM images of CoMoP@C with the carbon shell thickness of 2.6-3.8 nm.

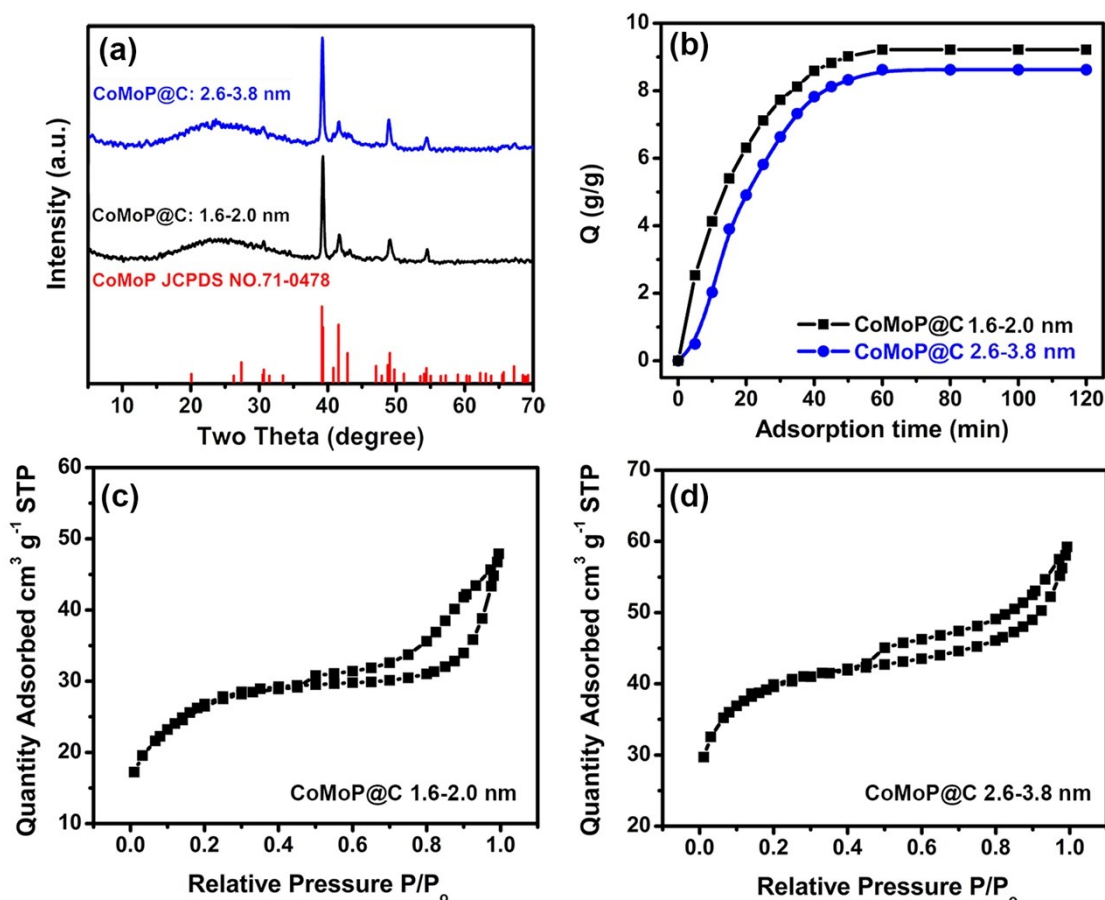


Figure S19. (a) The XRD patterns of CoMoP@C with the carbon shell thickness of 1.6-2.0 nm (black line) and CoMoP@C with the carbon shell thickness of 2.6-3.8 nm (blue line). (b) Dependence of adsorption time on the amounts of adsorbed H^+ on CoMoP@C with the carbon shell thickness of 1.6-2.0 nm, and CoMoP@C with the carbon shell thickness of 2.6-3.8 nm in 5 mM HCl aqueous solution. The maximum H^+ adsorption capacity (based on the quality of HCl) are about 8.63 and 9.36 g/g, respectively. (c) N_2 sorption isotherms of CoMoP@C with the carbon shell thickness of 1.6-2.0 nm. (b) N_2 sorption isotherms of CoMoP@C with the carbon shell thickness of 2.6-3.8 nm. The Brunauer-Emmett-Teller (BET) surfaces of CoMoP@C with 1.6-2.0 nm thick carbon shell and CoMoP@C with 2.6-3.8 nm thick carbon shell are 96 and 136 $m^2 g^{-1}$, respectively. Meanwhile, N_2 sorption isotherms indicate that these materials possess mesoporous structure.

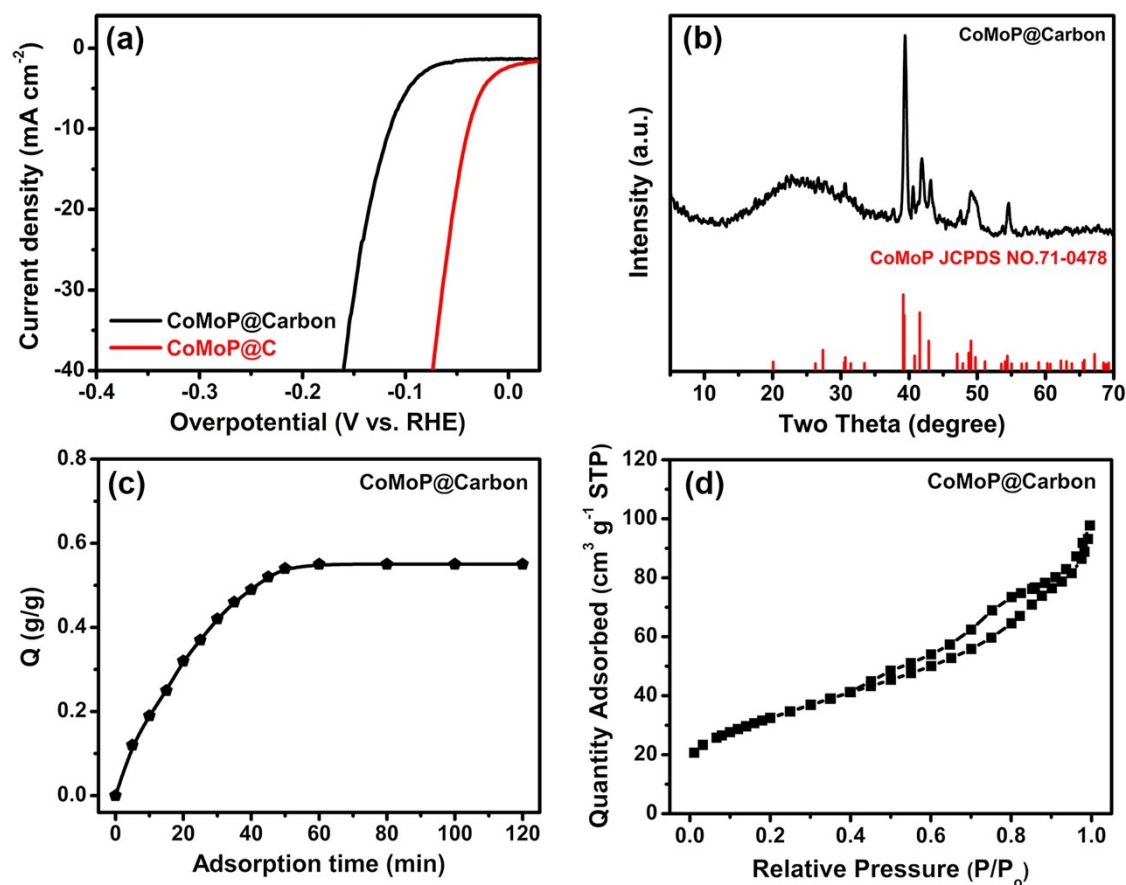


Figure S20. (a) The HER polarization curves of CoMoP@C and CoMoP@carbon (N free) in 0.5 M H₂SO₄ at scan rate of 5 mV s⁻¹. The activity of CoMoP@carbon (N-free) catalyst is inferior to that of CoMoP@C, which could be attributed to the N-dopants. (b) The XRD patterns of CoMoP NPs (black line) and CoMoP@carbon (N free) (blue line). The characteristic peaks located at 39.14°, 39.28°, 40.81°, 41.56°, 42.88°, 47.04°, 48.73°, 49.06°, 49.72° and 54.39° are also indexed to the (112), (210), (202), (211), (103), (013), (301), (020), (113) and (302) facets of orthorhombic CoMoP (JCPDS#71-0478). (c) Dependence of adsorption time on the amount of adsorbed H⁺ on CoMoP@carbon in 5 mM HCl aqueous solution. The maximum H⁺ adsorption capacity (based on the quality of HCl) is about 0.56g/g. (d) N₂ sorption isotherms of CoMoP@carbon. The Brunauer-Emmett-Teller (BET) surfaces area is 117 m² g⁻¹.

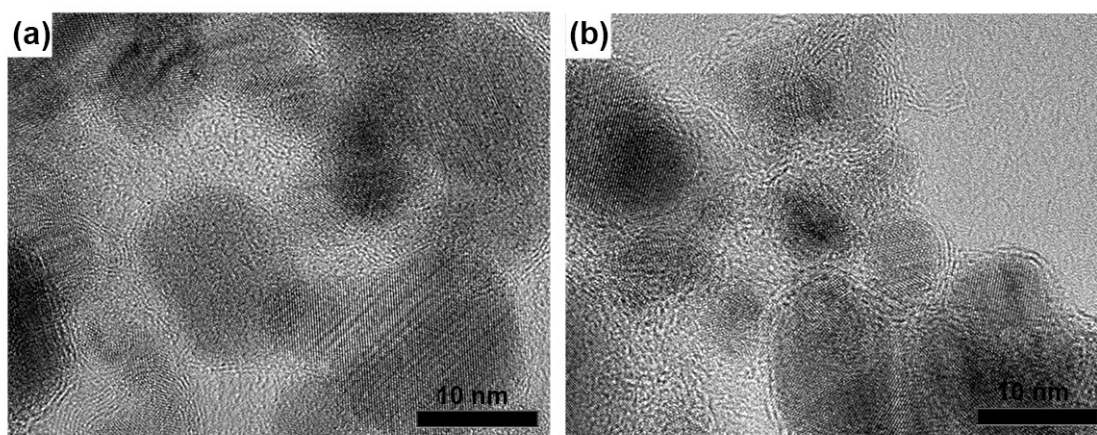


Figure S21. (a) and (b) The TEM images of CoMoP@carbon. The catalyst is also synthesized through a similar preparation procedure except that the dextran is used instead of DCA. The TEM images show that the CoMoP nanoparticles are also coated by multi-layer carbon shell.

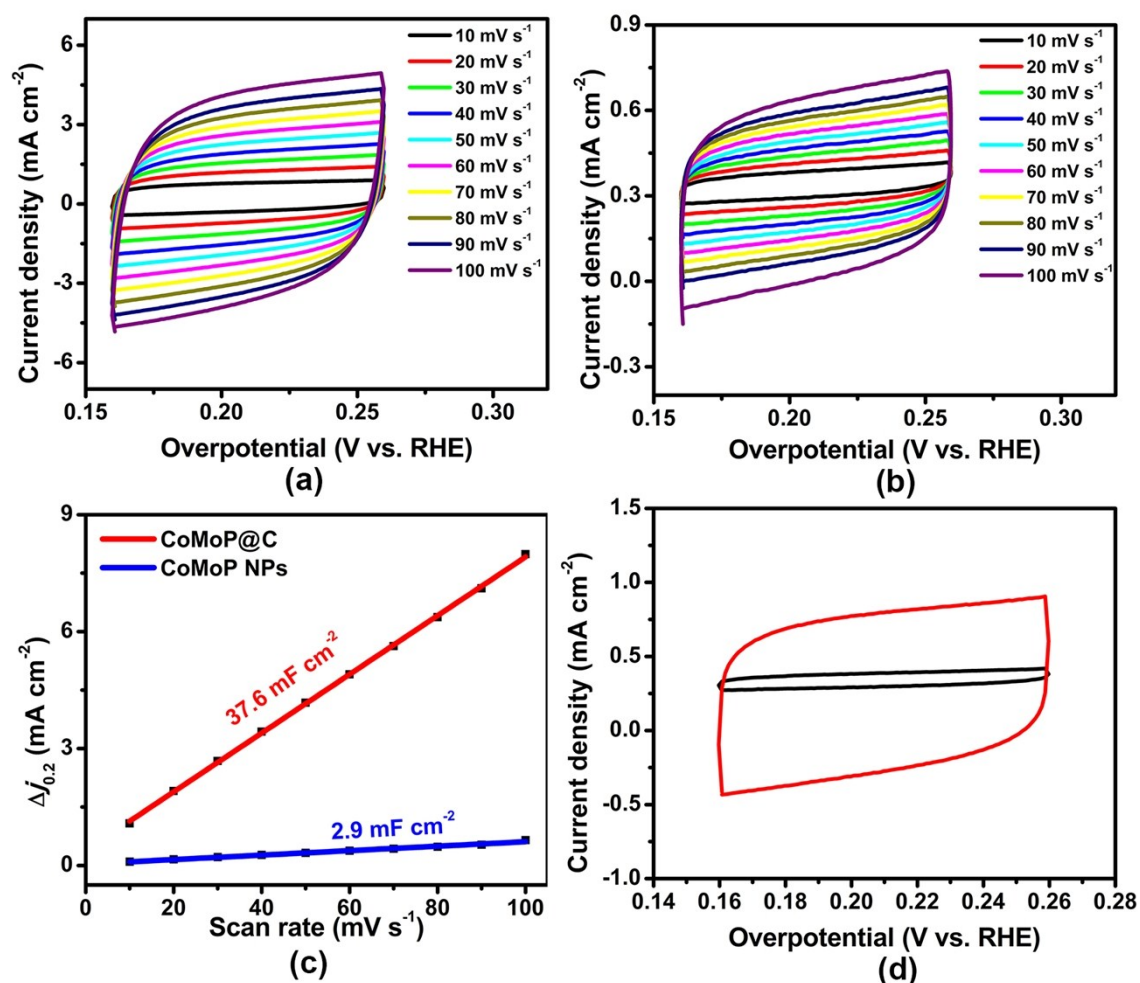


Figure S22. Cyclic voltammograms (CVs) of (a) CoMoP@C and (b) CoMoP NPs in the potential range from 0.16 to 0.26 V without redox current peaks in 0.5 M H₂SO₄; (c) Linear fitting of Δj of both samples ($\Delta j = j_a - j_c$) vs. scan rates at a given potential of +0.2 V vs. RHE.

j_a is the anodic current density and j_c is the cathodic current density, respectively; (d) Comparison of the CV curves of CoMoP@C and CoMoP NPs at 10 mV s^{-1} within the same potential region.

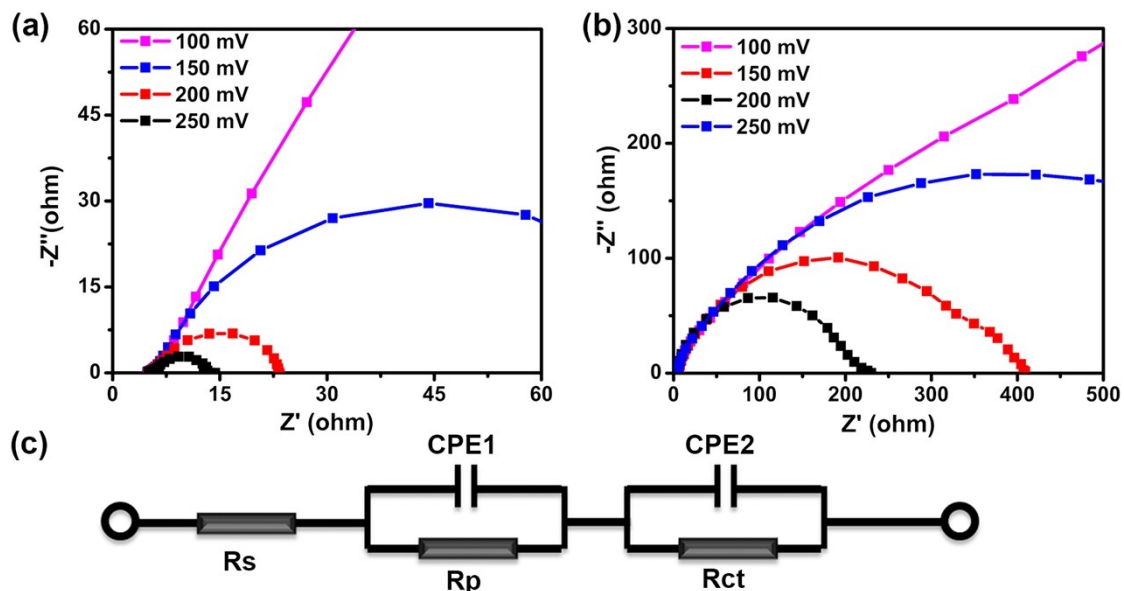


Figure S23. Nyquist plots of electrochemical impedance spectra (EIS) of (a) CoMoP@C and (b) CoMoP NPs recorded in $0.5 \text{ M H}_2\text{SO}_4$ aqueous solution. (c): Two-time-constant model equivalent circuit used for data fitting of EIS spectra (R_s represents the overall series resistance, CPE1 and CPE2 represent the constant phase element and resistance related to surface porosity R_p , and R_{ct} represents the charge transfer resistance related to HER process). As shown in Fig.S25, the charge transfer resistances (R_{ct}) of CoMoP@C sharply decrease with the increasing overpotential. The small R_{ct} values of CoMoP@C (6.5Ω in $0.5 \text{ M H}_2\text{SO}_4$) suggest that the catalyst exhibits fast electron transfer ability and higher catalytic activities for HER.

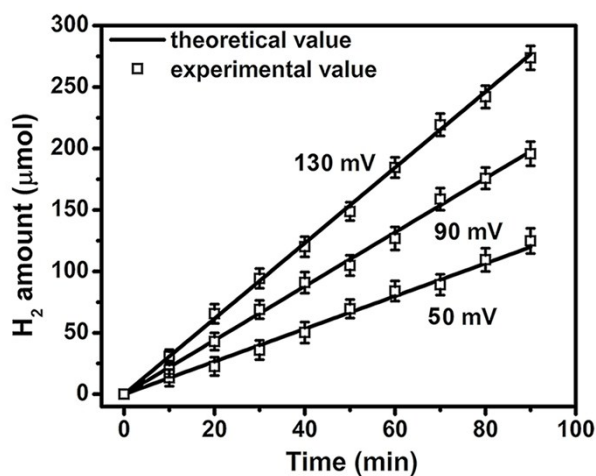


Figure S24. Faradaic Efficiency (FEs) of CoMoP@C toward HER in $0.5 \text{ M H}_2\text{SO}_4$ at different overpotentials during 90 min.

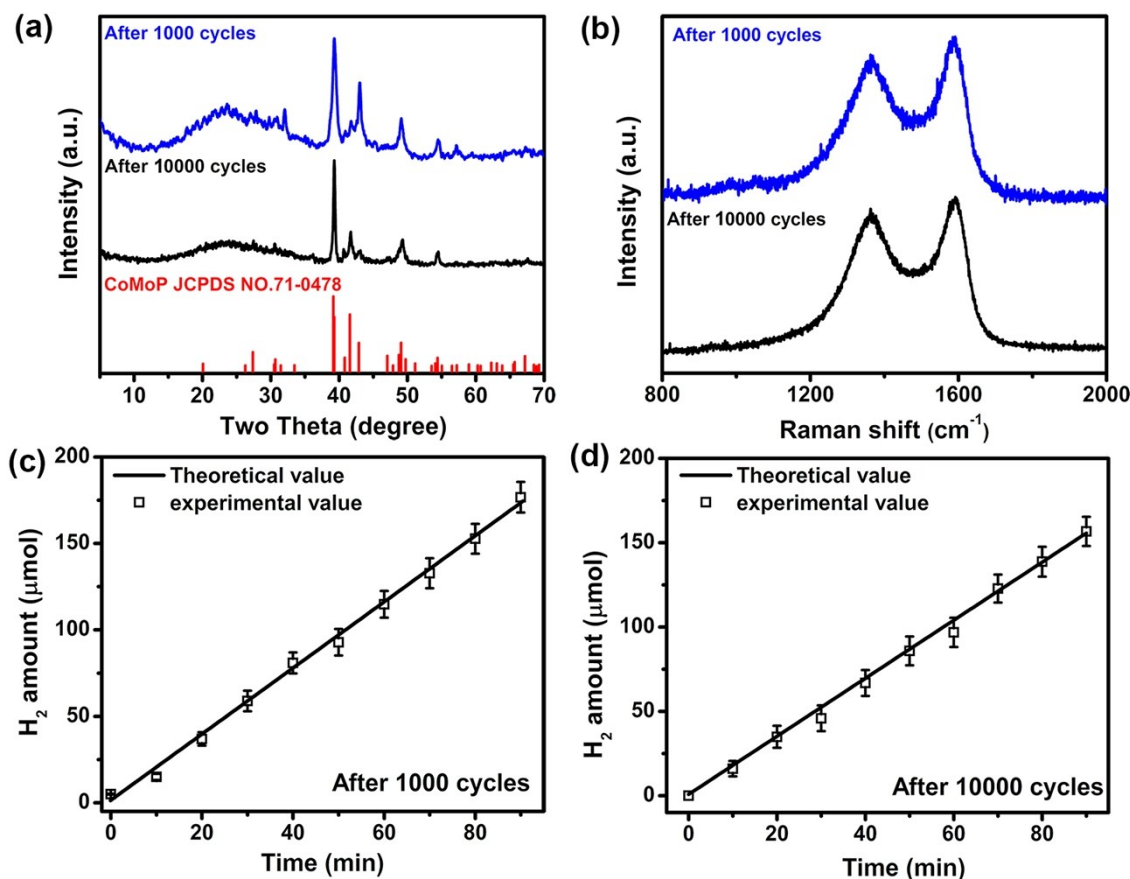


Figure S25. (a) The XRD patterns of CoMoP@C after 1000 cycles (blue line) and 10000 cycles (black line). (b) The Raman spectra of CoMoP@C after 1000 cycles (blue line) and 10000 cycles (black line). These results reveal that the structure of CoMoP@C could be remained after 10000 cycles HER test. (c) and (d) Faradiac efficiency of CoMoP@C toward HER in 0.5 M H₂SO₄ at the overpotential of 90 mV after 1000 cycles and 10000 cycles.

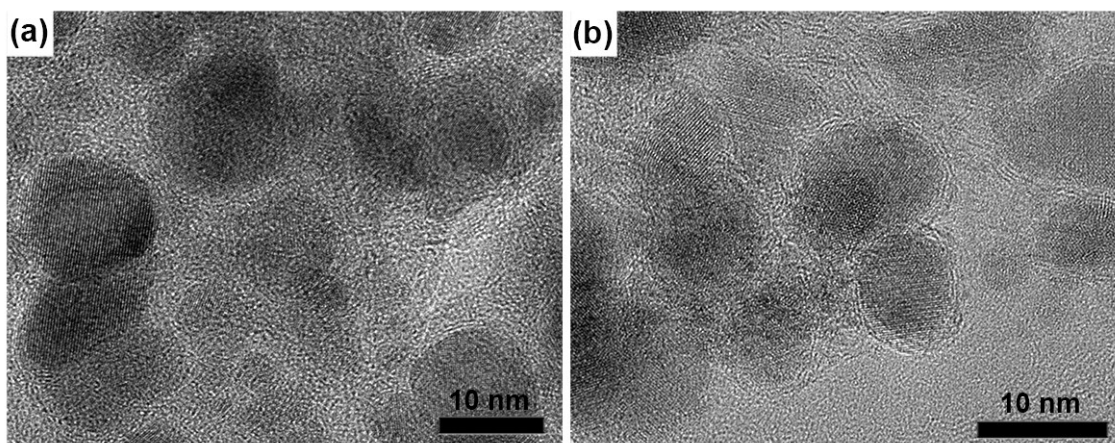


Figure S26. (a) and (b) TEM images of CoMoP@C after 10000 cycles test. The images show that the morphology of CoMoP@C catalyst shows negligible changes.

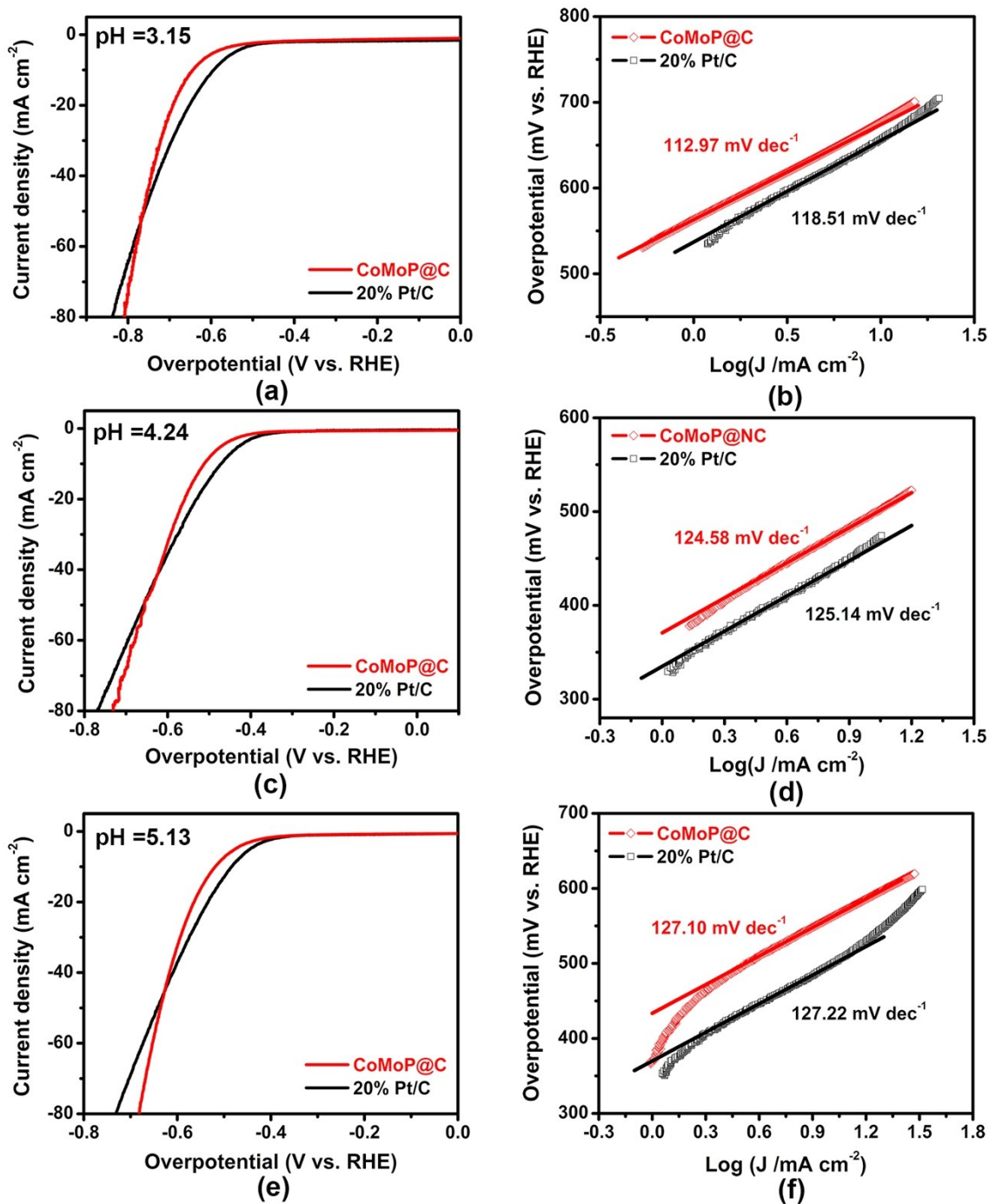


Figure S27. The HER polarization plots of CoMoP@C and commercial 20% Pt/C catalyst in pH 3.15 (a), 4.24 (c) and 5.13 (e) electrolytes at scan rate of 5 mV s⁻¹. (b), (d) and (f) The corresponding Tafel plots for CoMoP@C and Pt/C catalysts.

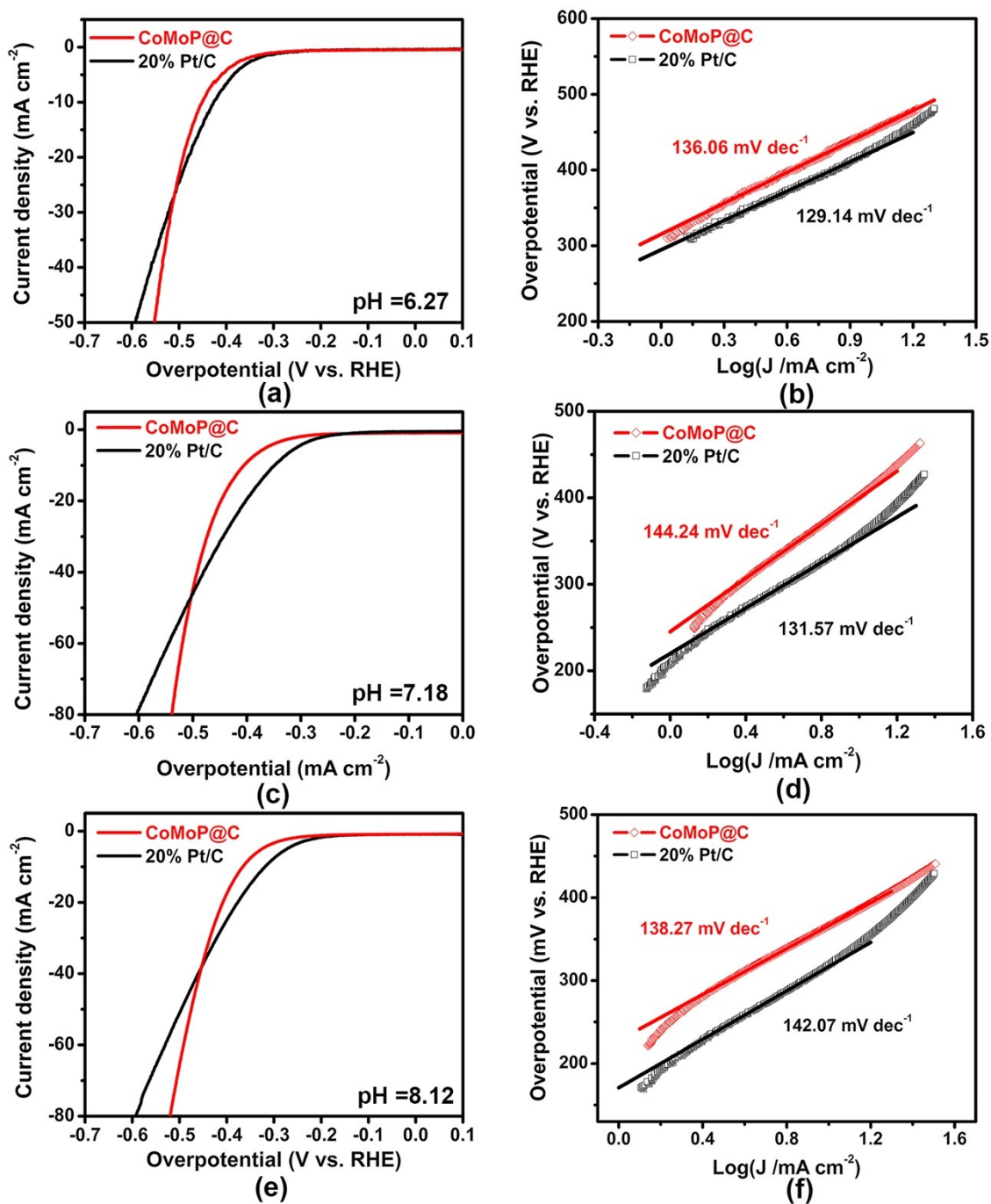


Figure S28. The HER polarization plots of CoMoP@C and commercial 20% Pt/C catalyst in pH 6.27 (a), 7.18 (c) and 8.12 (e) electrolytes at scan rate of 5 mV s⁻¹. (b), (d) and (f) the corresponding Tafel plots for CoMoP@C and Pt/C catalysts.

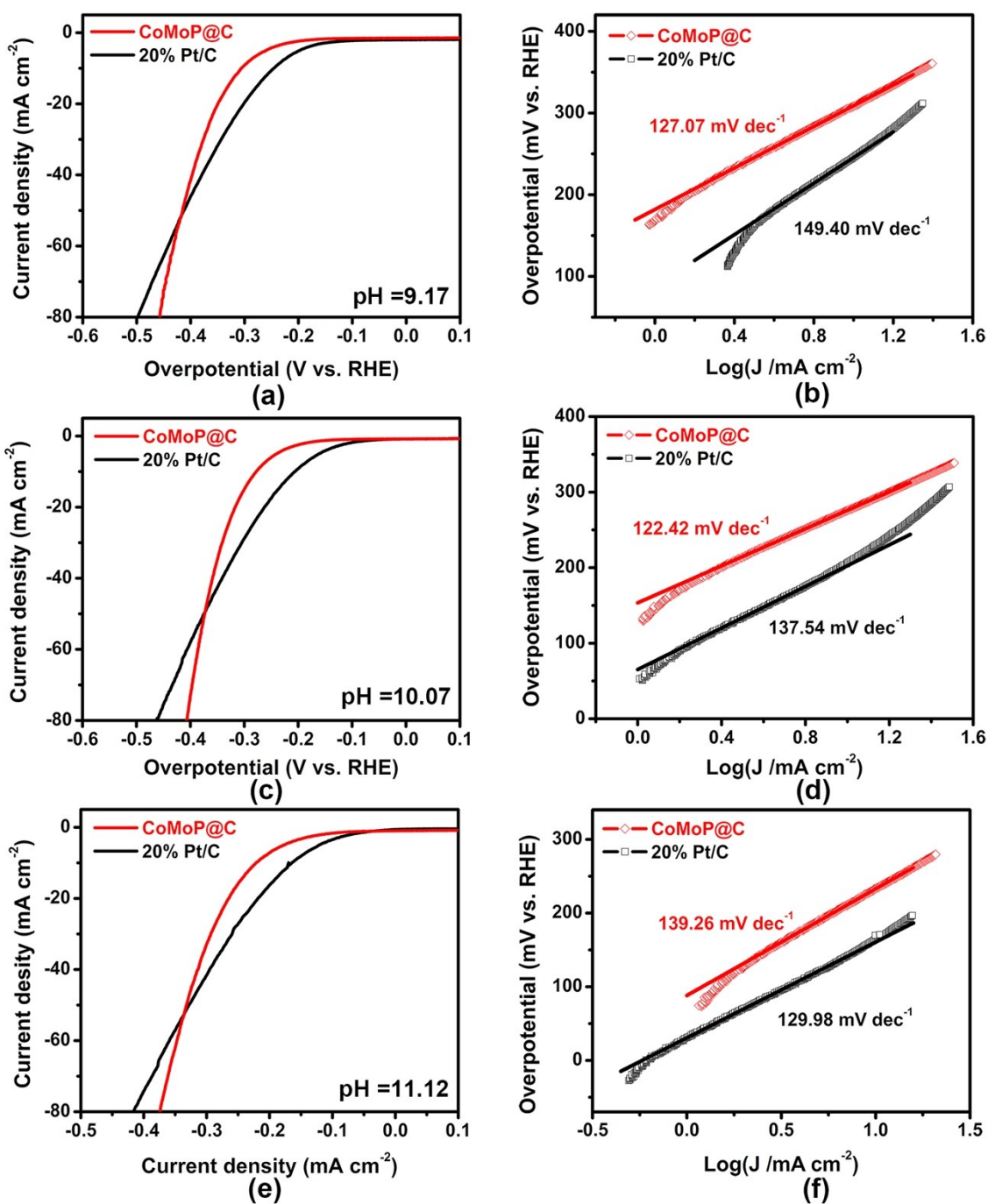


Figure S29. The HER polarization plots of CoMoP@C and commercial 20% Pt/C catalyst in pH 9.17 (a), 10.07 (c) and 11.12 (e) electrolytes at scan rate of 5 mV s⁻¹. (b), (d) and (f) the corresponding Tafel plots for CoMoP@C and Pt/C catalysts.

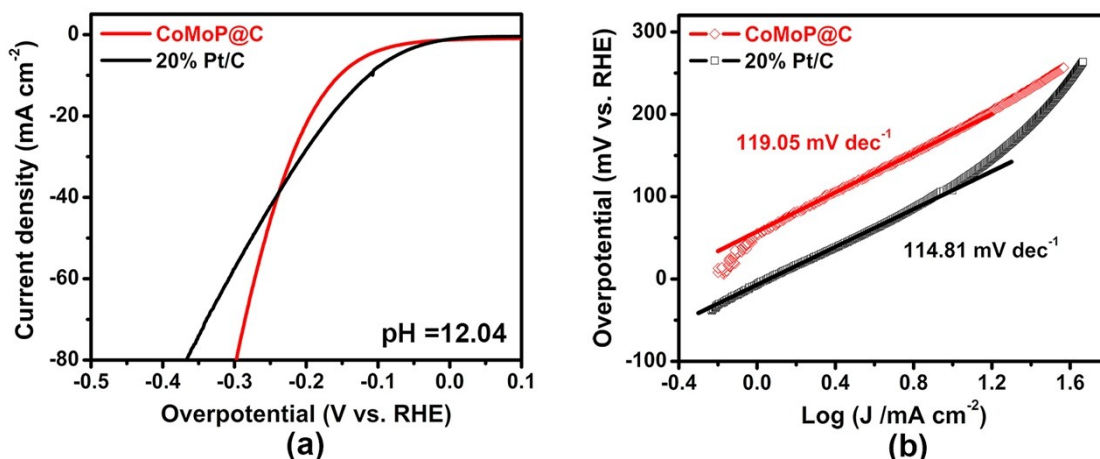


Figure S30. (a) The HER polarization plots of CoMoP@C and commercial 20% Pt/C catalyst in pH 12.04 at scan rate of 5 mV s^{-1} . (b) the corresponding Tafel plots for CoMoP@C and Pt/C catalysts.

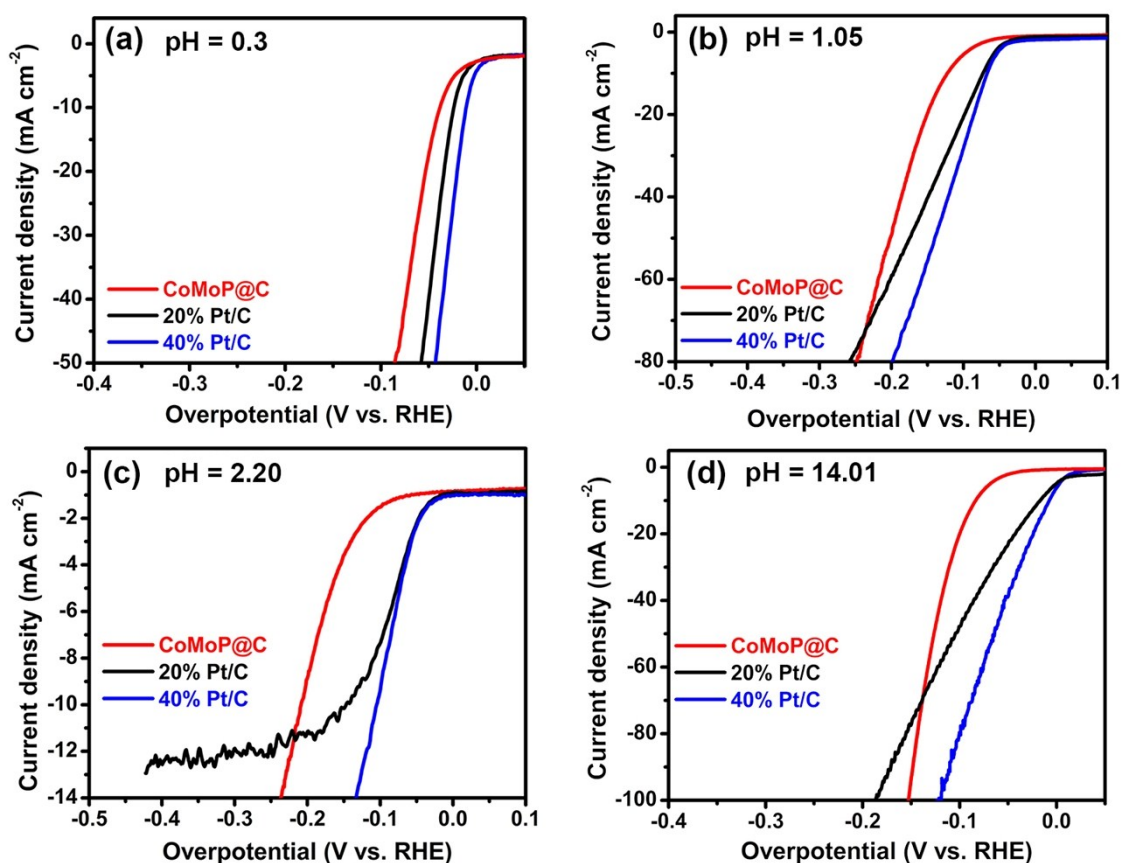


Figure S31. (a) The HER polarization plots of CoMoP@C, commercial 20% Pt/C and 40% Pt/C catalysts in pH 0.3 ($0.5 \text{ M H}_2\text{SO}_4$) electrolyte at scan rate of 5 mV s^{-1} . (b) The HER polarization plots of CoMoP@C, commercial 20% Pt/C and 40% Pt/C catalysts in pH 1.05 electrolyte at scan rate of 5 mV s^{-1} . (c) The HER polarization plots of CoMoP@C, commercial 20% Pt/C and 40% Pt/C catalysts in pH 2.20 electrolyte at scan rate of 5 mV s^{-1} . (d) The HER polarization plots of CoMoP@C, commercial 20% Pt/C and 40% Pt/C catalysts in pH 14.01 electrolyte at scan rate of 5 mV s^{-1} .

(d) The HER polarization plots of CoMoP@C, commercial 20% Pt/C and 40% Pt/C catalysts in pH 14.01 electrolyte at scan rate of 5 mV s^{-1} .

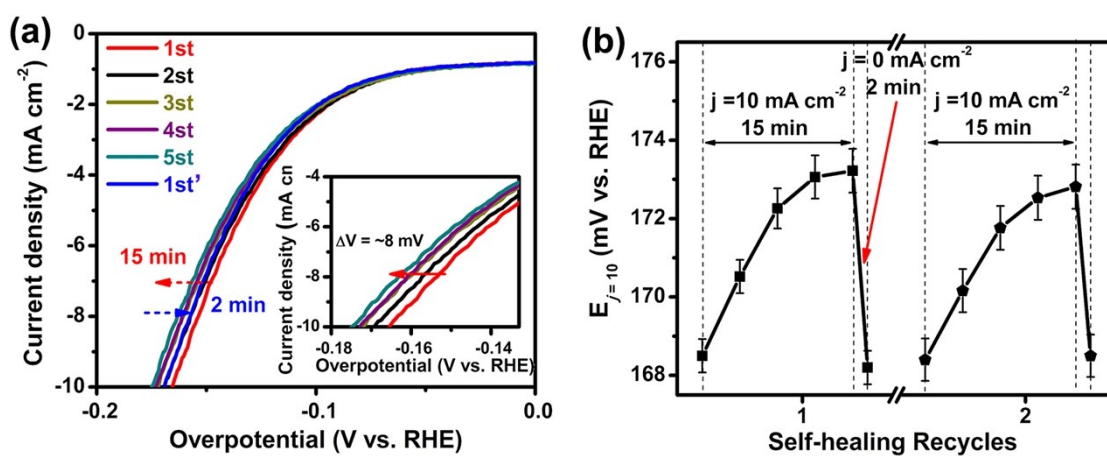


Figure S32. (a) Polarization curves of CoMoP@C in pH 2.20 electrolyte at scan rate of 5 mV s^{-1} during 17 min test. Red line represents the first scan of catalyst. Blue line represents the first scan after the potential is off for 2 min. (b) The variation of overpotential at current density of 10 mA cm^{-2} during 17 min for 2 recycles.

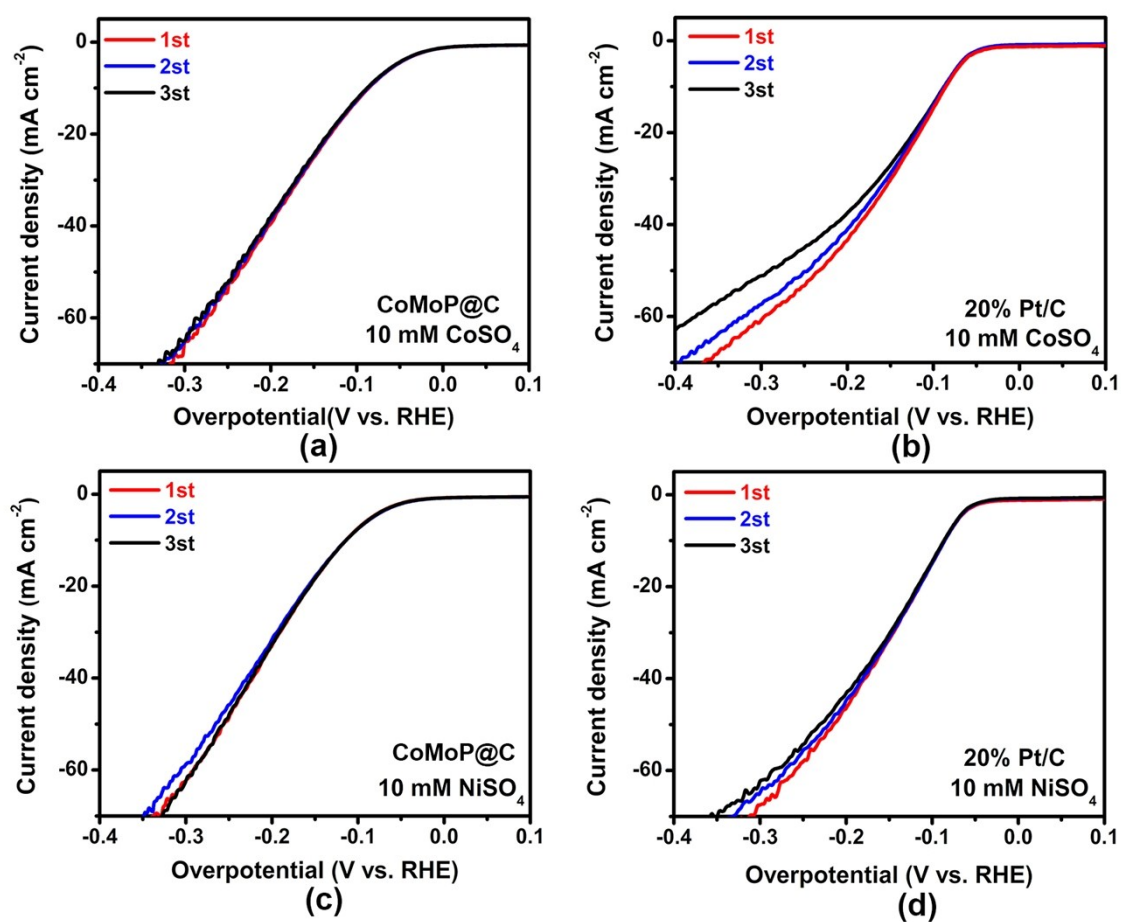


Figure S33. (a) and (b) The HER polarization curves of CoMoP@C and 20% Pt/C in pH 1.05 electrolyte with 10 mM CoSO₄. (c) and (d) The HER polarization curves of CoMoP@C and 20% Pt/C in pH 1.05 electrolyte with 10 mM NiSO₄.

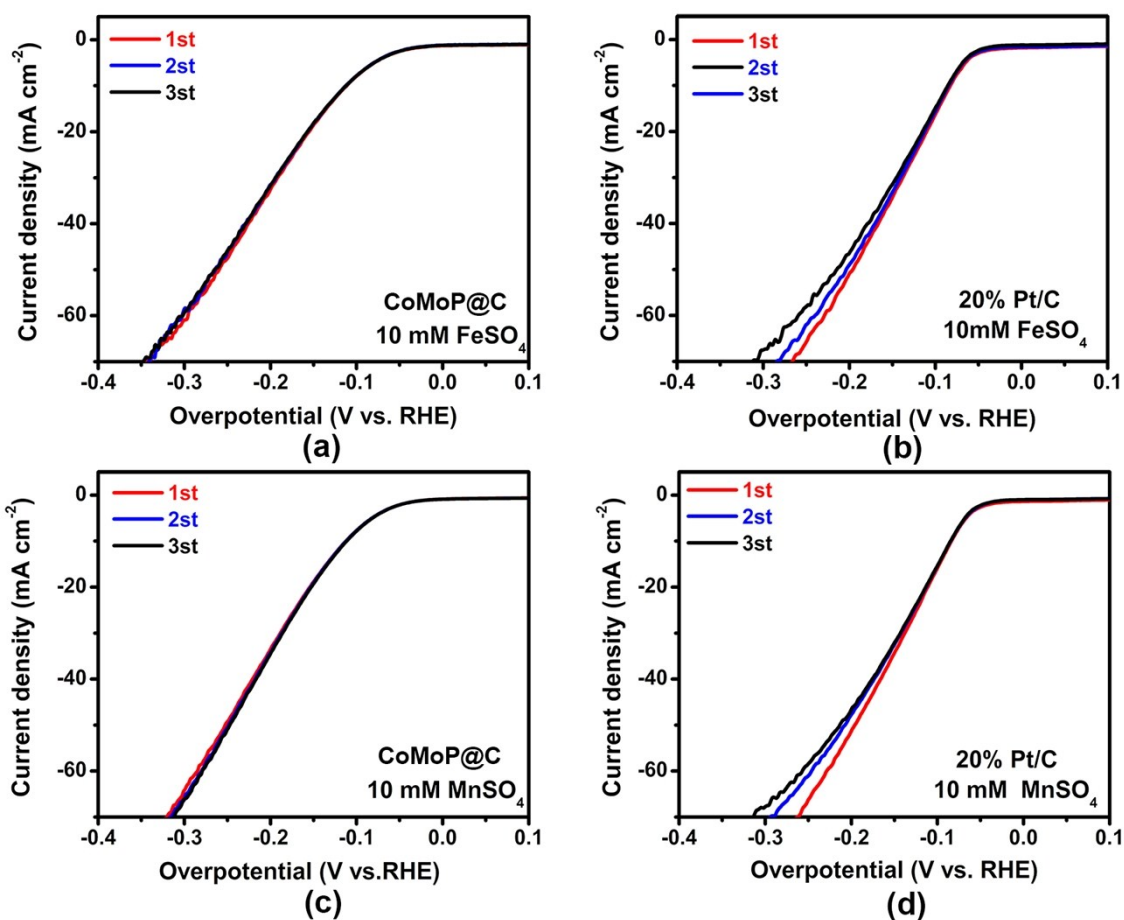


Figure S34. (a) and (b) The HER polarization curves of CoMoP@C and 20% Pt/C in pH 1.05 electrolyte with 10 mM FeSO₄. (c) and (d) The HER polarization curves of CoMoP@C and 20% Pt/C in pH 1.05 electrolyte with 10 mM MnSO₄. Figure S32 and S33 show that the activity of CoMoP@C catalyst almost remains unchanged in the presence of Co²⁺, Ni²⁺, Fe²⁺ and Mn²⁺, while the activity of Pt/C has certain reduction after 3 cycles, indicating the presence of transition metals might have influence on the activity of Pt/C.

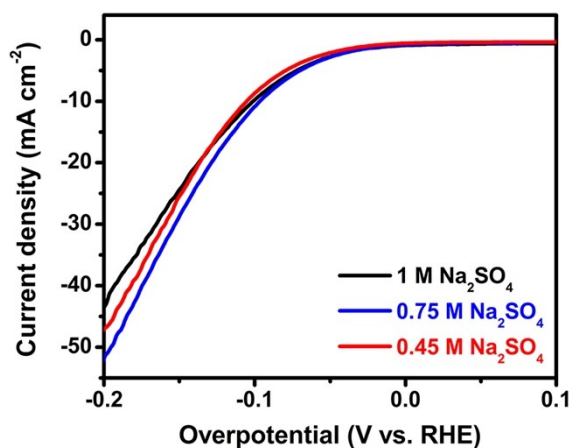


Figure S35. The HER polarization curves of CoMoP@C in pH 1.05 electrolyte with different concentration of supporting electrolyte Na₂SO₄. The result shows that the current density of

catalyst will increase as the concentration of supporting electrolyte increases, while the amount of supporting electrolyte is too much, the activity of catalyst will decrease, which could be attributed to the competition of Na^+ and H^+ on the surface of catalyst.

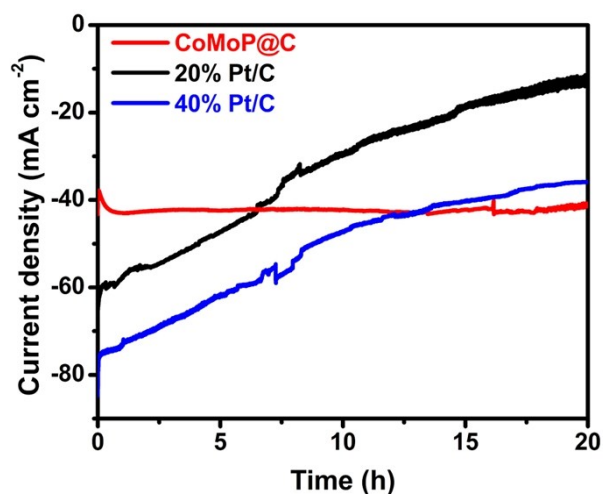


Figure S36. Time-dependent current density curve of CoMoP@C, 20% and 40% Pt/C under a static overpotential of 600 mV for 20 h in simulated seawater. The HER activity of CoMoP@C is higher than that of 20% Pt/C (40% Pt/C) in real seawater after 6 h (13 h) reaction.

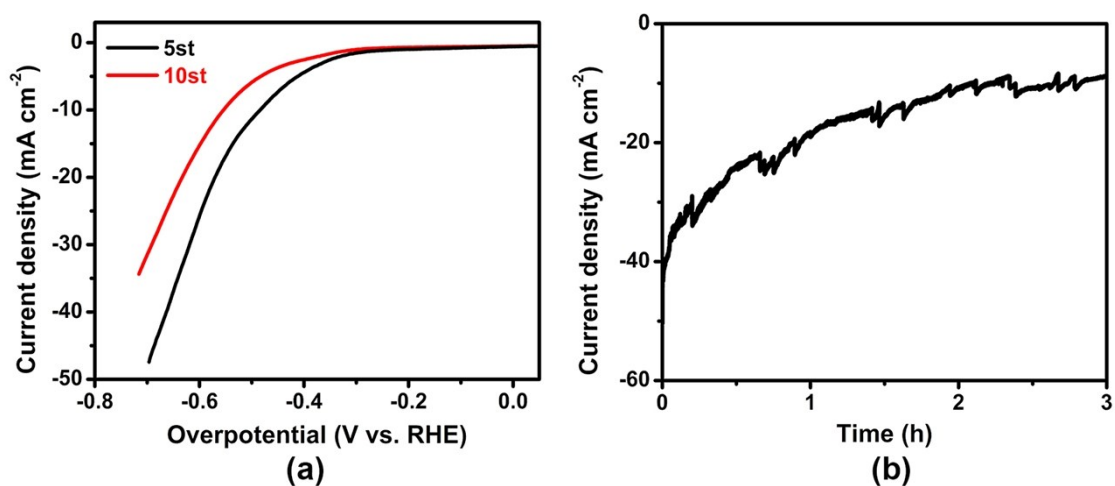


Figure S37. (a) The HER polarization plots of CoMoP NPs in seawater at scan rate of 5 mV s^{-1} in 5st and 10st test. (b) Time-dependent current density curve of CoMoP NPs under a static overpotential of 670 mV for 3 h in seawater. The current density of CoMoP NPs drops over 75% in three hours.

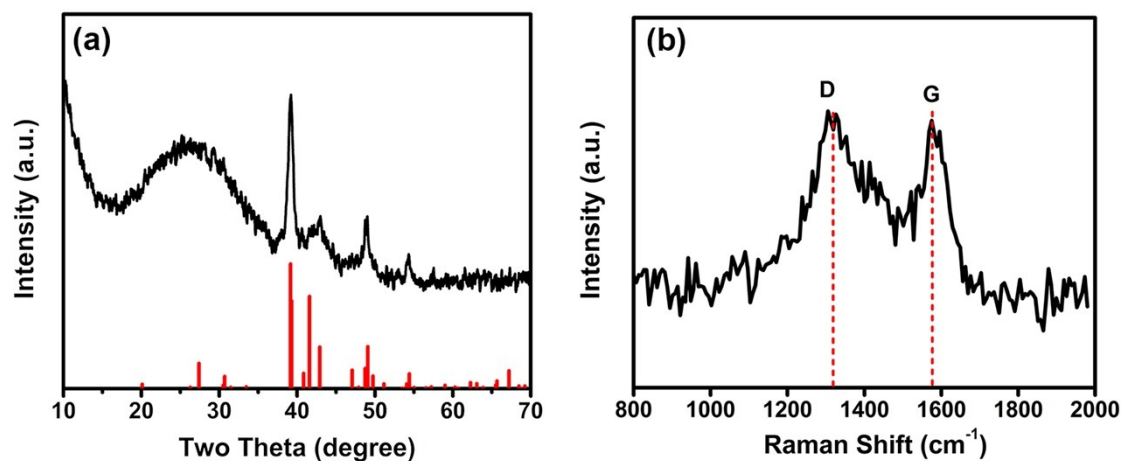


Figure S38. (a) The XRD patterns of CoMoP@C after HER test in real seawater. (b) The Raman spectra of CoMoP@C after HER test in real seawater. These results reveal that the structure of CoMoP@C could be remained in seawater.

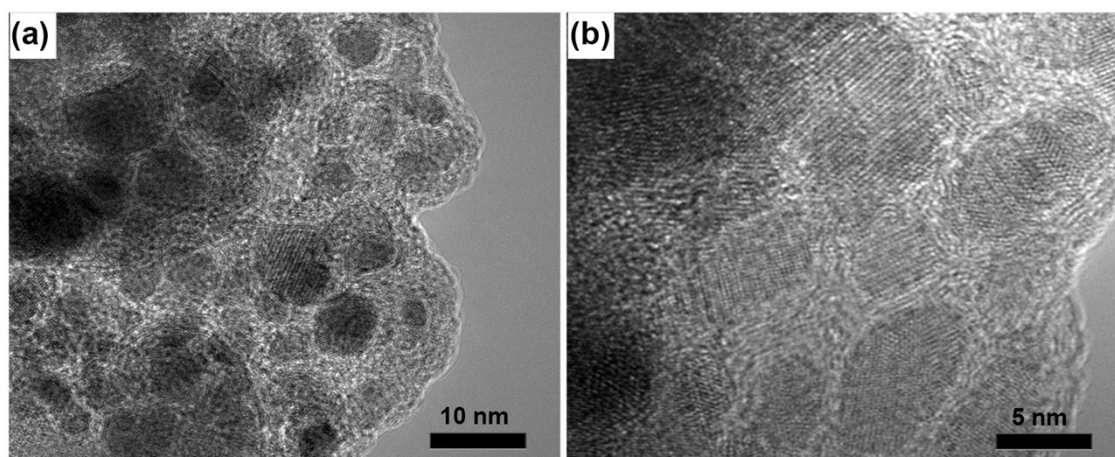


Figure S39. (a) and (b) The TEM images of CoMoP@C after HER test in real seawater. The images show that the morphology of catalyst almost keeps unchanged.

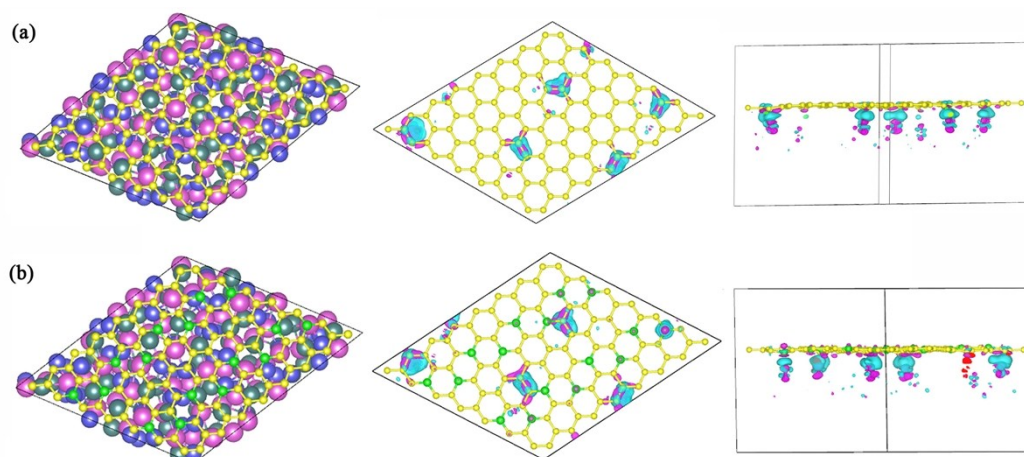


Figure S40. Models of the structures of CoMoP@Carbon (without N dopants) and CoMoP@C (with N dopants), and their charge density difference $\Delta\rho$ with the pink and blue areas denoting low and high charge density, respectively (top and side views of the adsorption sites). The yellow, green, violet, blueviolet, and darkcyan balls represent C, N, P, Co and Mo atoms, respectively. The results indicate that the carbon atoms adjacent to N atom in CoMoP@C could possess considerably high activity for HER, which are corresponding to the blue area in the CDD picture of CoMoP@C.

Table S1. The lattice parameters (\AA) of the supercells for all the systems

Models	a	b	c
C	14.76	14.76	18.00
N-doped C shell	17.08	19.54	18.00
CoMoP	18.07	19.11	18.00
CoMoP@carbon	17.64	19.58	18.00
CoMoP@C	17.53	19.43	18.00

Table S2. The $\Delta E(\text{H}^*)$, $ZPE(\text{H}^*)$ and $\Delta G(\text{H}^*)$ values of the H^* adsorbed on different surfaces

Models	$\Delta E(\text{H}^*)/\text{eV}$	$ZPE(\text{H}^*)/\text{eV}$	$\Delta G(\text{H}^*)/\text{eV}$
C	1.483	0.301	1.832
N-doped C shell	0.821	0.289	1.181
CoMoP	-0.822	0.195	-0.555
CoMoP@carbon	0.050	0.312	0.434
CoMoP@C	-0.276	0.307	0.103

Table S3. The C, N, O, Co, Mo, and P components of CoMoP@C recorded from the EDX quantitative analyses

Element	Percentage by weight /%	Percentage by atoms /%
C K	19.38	52.55
N K	0.54	1.23
O K	2.56	5.21
Co K	24.47	13.51
Mo L	39.67	13.45
P K	13.38	14.05

Table S4. The C, N, O, Co, Mo, and P components of CoMoP@C obtained from the XPS analyses

Element	Percentage by atoms /%
C	50.17
N	10.11
O	30.37
Co	3.49
Mo	2.14
P	2.73

The elemental analysis from XPS indicates that the catalyst is composed of Co, Mo, P, C, N and O elements. The high content of O element could be attributed to the surface oxidation.

Table S5. The ICP result of CoMoP@C

Element	Content /(mg/kg)
Co	2.52×10^5
Mo	3.89×10^5
P	1.37×10^5

The result of ICP is consistent with the EDX result.

Table S6. The C, N, O, Co, Mo, and P components of N-doped C shell recorded from the EDX quantitative analyses

Element	Percentage by weight /%	Percentage by atoms /%
C K	67.99	74.89
N K	6.55	6.19
O K	21.98	18.17
Co K	0.57	0.13
Mo L	2.16	0.3
P K	0.75	0.32

Table S7. The value of charge transfer resistance (R_{ct}) and a series resistance (R_s) for CoMoP@C with overpotential from 100 to 250 mV in 0.5 M H₂SO₄.

Potential (mV vs. RHE)	CoMoP@C		CoMoP NPs	
	R_{ct} (Ω)	R_s (Ω)	R_{ct} (Ω)	R_s (Ω)
100	538.2	5.88	8584	5.68
150	62.58	5.54	1374	5.58
200	15.32	5.26	631.8	5.33
250	6.53	5.28	258.5	5.01

Table S8. Summary of HER activity of CoMoP@C, 20% Pt/C and 40% Pt/C catalyst in the electrolytes with different pH

pH of Electrolyte	Overpotential at current density of 50 mA cm ⁻² (mV vs. RHE)		
	CoMoP@C	20% Pt/C	40% Pt/C
0.3	96.2	58.2	43.3
1.05	220.4	201.6	174.9
3.15	761.3	767.4	676.2
4.24	670.1	677.5	607.8
5.13	630.8	654.3	575.8
6.27	574.5	592.2	510.5
7.18	525.7	542.2	441.7
8.12	486.4	497.1	403.4
9.17	421.1	413.7	371.1
10.07	375.2	374.8	328.3
11.12	312.3	310.7	268.1
12.04	267.9	276.6	232.1
13.11	212.3	216.4	137.2
14.01	136.9	105.3	76.7

Note: all values in this table are average values for five times tests.

Table S9. Comparison of HER performance in acidic media for CoMoP@C with other HER electrocatalysts.

Catalyst	Current density (mA cm ⁻²)	Overpotential (mV)	Tafel slope (mV dec ⁻¹)	J_o (mA cm ⁻²)	Ref.
CoMoP@C	10	41	49.73	1.21	This work
CoP/CC	10	67	51	0.288	<i>J. Am. Chem. Soc.</i> 2014, 136, 7587
CoP NWs	10	110	54	0.15	<i>J. Mater. Chem. A.</i> 2014, 2, 14634
CoP/CNT	10	122	54	0.13	<i>Angew. Chem. Int. Ed.</i> 2014, 53, 6710
MoP@PC	10	153	66	0.21	<i>Angew. Chem. Int. Ed.</i> 2016, 55, 12854
CoPS NPI	10	48	56	0.984	<i>Nat. Mater.</i> 2015, 14, 1245
CoP/rGO-400	10	105	50	N.A.	<i>Chem. Sci.</i> 2016, 7, 1690
CoNiP@NF	10	60	39	0.54	<i>J. Mater. Chem. A.</i> 2016, 4, 10195
CoP CPH	10	133	51	0.044	<i>J. Mater. Chem. A.</i> 2015, 3, 21471
MoP	10	150	50	0.01	<i>J. Mater. Chem. A.</i> 2015, 3, 4368
MoP-CA2	10	125	54	0.086	<i>Adv. Mater.</i> 2014, 26, 5702
3D MoP	10	105	126	3.052	<i>J. Mater. Chem. A.</i> 2016, 4, 59
Co-MoP	10	215	50	0.071	<i>Catal. Sci. Technol.</i> 2016, 6, 1952
Fe-CoP/Ti	10	78	75	N. A.	<i>Adv. Mater.</i> 2016, DOI: 10.1002/adma.201602441
NiP _{1.93} Se _{0.07} /CP	10	84	41	0.1	<i>ACS. Catal.</i> 2015, 5, 6355
Mo-W-P/CC	100	138	52	0.288	<i>Energy Environ. Sci.</i> 2016, 9, 1468

Table S10. Comparison of HER performance in alkaline media for CoMoP@C with other HER electrocatalysts.

Catalyst	Current density (mA cm ⁻²)	Overpotential (mV)	Tafel slope (mV dec ⁻¹)	J_0 (mA cm ⁻²)	Ref.
CoMoP@C	10	81	55.5	0.26	This work
CoP-MNA	10	54	51	0.857	<i>Adv. Funct. Mater.</i> 2015, 25, 7337
CoP/CC	10	209	129	N.A.	<i>J. Am. Chem. Soc.</i> 2014, 136, 7587
CoP film	10	94	42	N.A.	<i>Angew. Chem. Int. Ed.</i> 2015, 54, 6251
Co _{0.59} Fe _{0.41} P	10	92	72	0.568	<i>Nanoscale.</i> 2015, 7, 11055
CoP/rGO-400	10	150	38	N.A.	<i>Chem. Sci.</i> 2016, 7, 1690
CoP NRs	20	171	N.A.	N.A.	<i>Nano Energy.</i> 2014, 9, 373
MoP/NP-CNT	10	117	58	0.1	<i>RSC Adv.</i> 2016, 6, 7370
MoP	30	180	48	0.046	<i>Energy Environ. Sci.</i> 2014, 7, 2624
CoNiP@NF	10	155	134	N.A.	<i>J. Mater. Chem. A.</i> 2016, 4, 10195
Ni ₅ P ₄ MPs	10	49	98	N.A.	<i>Energy Environ. Sci.</i> 2015, 8, 1027
Ni ₂ P/Ni/NF	10	98	72	0.845	<i>ACS Catal.</i> 2016, 6, 714
Ni ₂ P-G@NF	10	50	30	N.A.	<i>J. Mater. Chem. A.</i> 2015, 3, 1941
Co-Ni-P-300	10	150	60.6	N.A.	<i>Chem. Commun.</i> 2016, 52, 1633

Supplementary References

- [1] H. Miao, H. X. Wan, M. Liu, Y. Zhang, X. Xu, W. W. Ju, D. R. Zhu, Y. Xu, *J. Mater. Chem. C*, 2014, **2**, 6554.
- [2] H. Li, W. Q. Kong, J. Liu, N. Y. Liu, H. Huang, Y. Liu, Z. H. Kang, *Carbon*, 2015, **91**, 66.
- [3] A. Laisa, in *Handbook of Fuel Cells* (Eds.: W. Vielstich, H. A. Gasteiger, A. Lamm, H. Yokokawa). Wiley 2010.
- [4] Y. Zheng, Y. Jiao, M. Jaroniec, S. Z. Qiao, *Angew. Chem. Int. Ed.*, 2015, **54**, 52.
- [5] S. J. Clouser, J. C. Huang, E. Yeager, *J. Appl. Electrochem.*, 1993, **23**, 597.
- [6] T. Shinagawa, A. T. Garcia-Esparza, K. Takanahe, *Sci. Rep.*, 2015, **5**, 13801.
- [7] J. K. Nørskov, T. Bligaard, A. Logadottir, J. R. Kitchin, J. G. Chen, S. Pandelov, U. Stimming, *J. Electrochem. Soc.*, 2005, **152**, J23.
- [8] G. Kresse, J. Hafner, *J. Phys. Rev. B*, 1993, **47**, 558.
- [9] G. Kresse, J. Hafner, *J. Phys. Rev. B*, 1994, **49**, 14251.
- [10] J. P. Perdew, K. Burke, M. Ernzerhof, *Phys. Rev. Lett.*, 1996, **77**, 3865.
- [11] P. E. Blöchl, *Phys. Rev. B*, 1994, **50**, 17953.
- [12] G. Kresse, D. Joubert, *Phys. Rev. B*, 1999, **59**, 1758.
- [13] P. R. Guérin, *Acta Crystallogr., Sec. B*, 1978, **34**, 3312.
- [14] Y. P. Liu, G. T. Yu, G. D. Li, Y. H. Sun, T. Asefa, W. Chen, X. X. Zou, *Angew. Chem. Int. Ed.*, 2015, **54**, 10752.
- [15] G. Henkelman, A. Arnaldsson, H. Jónsson, *Comput. Mater. Sci.*, 2006, **36**, 354.

Additional experimental data:

To gain more insight to the electrocatalytic activity of CoMoP@C for HER, we prepared MoP catalyst for comparison. The precursor was prepared by the mixture of $(\text{NH}_4)_6\text{Mo}_7\text{O}_{24}\cdot 4\text{H}_2\text{O}$ and H_3PO_4 in aqueous solution with the molar ratio of Mo:P = 1:1.2, and then the solution was evaporated to dryness. The as-prepared precursor was mixed with DCA and annealed under the same condition as CoMoP@C prepared. The hexagonal phase MoP is obtained. The XRD patterns and HER performance of MoP are shown in Figure S41 and S42.

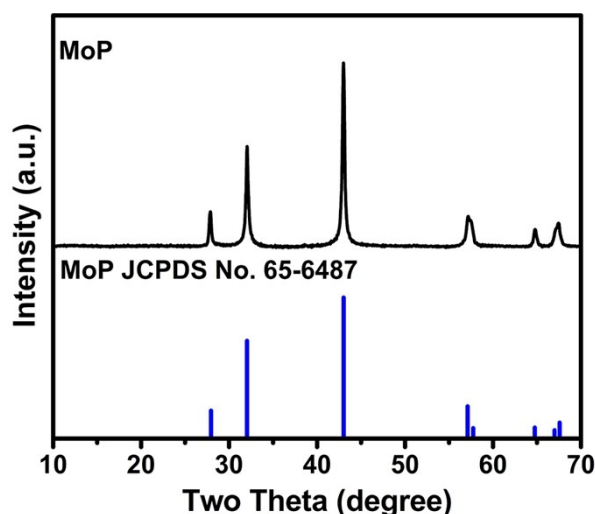


Figure S41. The XRD patterns of MoP. The characteristic peaks located at 27.93° , 32.04° , 43.02° and 57.11° are indexed to the (001), (100), (101), and (110) facets of hexagonal MoP (JCPDS#65-6487).

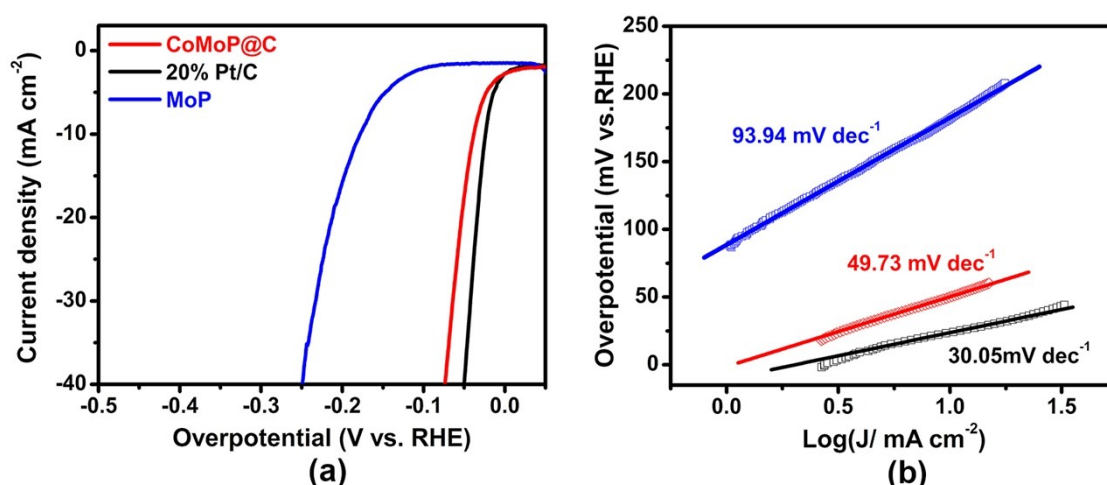


Figure S42. (a) The HER polarization plots of MoP, CoMoP@C and commercial 20% Pt/C catalyst in 0.5 M H_2SO_4 at scan rate of 5 mV s^{-1} . (b) the corresponding Tafel plots for MoP, CoMoP@C and Pt/C catalysts. The MoP shows an overpotential of 179 mV at a current density of 10 mA cm^{-2} , which is inferior to that of CoMoP@C.

Nickel is typically used in commercial alkaline electrolysis. We measured the HER performance of Nickel foam in 1 M KOH and seawater for comparison. The obtained results have been shown in Figure S43 and S44. As shown in Figure S43, Nickel foam needs an overpotential of 243 mV to afford a current density of 10 mA cm⁻², which is higher than that of CoMoP@C (83 mV). The HER activity of Nickel foam in seawater is also inferior to that of CoMoP@C.

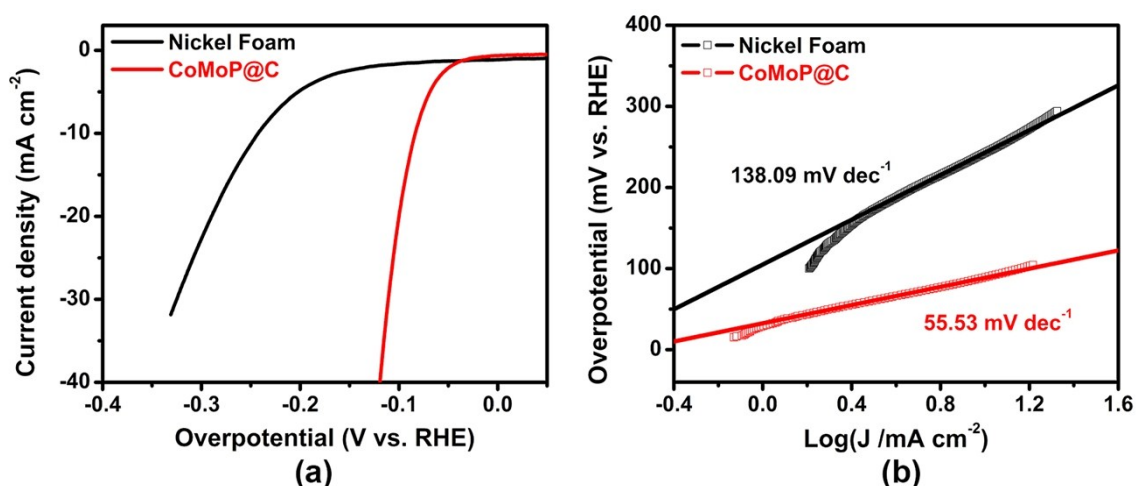


Figure S43. (a) The HER polarization plots of CoMoP@C and commercial Nickel Foam in 1 M KOH at scan rate of 5 mV s⁻¹. (b) the corresponding Tafel plots for CoMoP@C and commercial Nickel Foam. Although the Nickel foam is typically used in commercial alkaline electrolysis, the HER activity of Nickel foam is inferior than that of CoMoP@C, which needs an overpotential of 243 mV to afford a current density of 10 mA cm⁻².

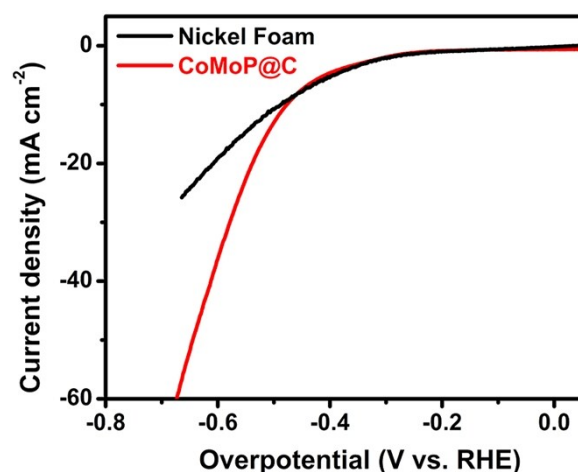


Figure S44. The HER polarization plots of CoMoP@C and commercial Nickel Foam in seawater at scan rate of 5 mV s⁻¹.